1 2 9 0

UNIVERSIDADE DE
COIMBRA

Joana Filipa Figueiredo Simão

# SMART DELIVERING AND DRUG TARGETING TO TREAT FIBROSIS IN AGE-RELATED MACULAR DEGENERATION

**Dissertation presented to University of Coimbra as a requirement for the degree of MSc in Medicinal Chemistry and performed under the supervision of Doctor Rosa Cristina Simões Fernandes, Auxiliary Investigator at the Faculty of Medicine of University of Coimbra, and Doctor João Paulo Tomé, Associate Professor at Instituto Superior Técnico of University of Lisbon**

May, 2021

Joana Filipa Figueiredo Simão

# SMART DELIVERING AND DRUG TARGETING TO TREAT FIBROSIS IN AGE-RELATED MACULAR DEGENERATION

Dissertation presented to University of Coimbra as a requirement for the degree of MSc in Medicinal Chemistry and performed under the supervision of Doctor Rosa Cristina Simões Fernandes, Auxiliary Investigator at the Faculty of Medicine of University of Coimbra, and Doctor João Paulo Tomé, Associate Professor at Instituto Superior Técnico of University of Lisbon

University of Coimbra

May, 2021

# Support

This work was conducted at the Coimbra Institute for Clinical and Biomedical Research (iCBR), Faculty of Medicine, University of Coimbra, Portugal in collaboration with the Centro de Química Estrutural, Departamento de Engenharia Química, Instituto Superior Técnico, Universidade de Lisboa.

The presented work was supported by Programa Operacional Factores de Competitividade COMPETE2020 (CENTRO-01-0145-FEDER-000008: BRAINHEALTH 2020) and by National funds via Portuguese Science and Technology Foundation (FCT): Strategic Projects UID/NEU/04539/2019 (CNC.IBILI), UIDB/04539/2020, UIDP/04539/2020 (CIBB), as well as by COMPETE-FEDER funds (POCI-01-0145-FEDER-007440).

*Progress is made by trial and failure; the failures are generally a hundred times more numerous than the successes; yet they are usually left unchronicled.*

*William Ramsay*

# Agradecimentos

O alcançar desta etapa não teria sido possível sem o carinho, auxílio e dedicação por parte de várias pessoas ao longo de todo o percurso da minha formação. Por esta razão, não quero deixar de agradecer a todos aqueles que, direta ou indiretamente, contribuíram para a realização desta tese.

À Doutora Rosa Fernandes, pela sua orientação, ensinamentos e pela oportunidade de realizar este trabalho. Pelo seu incentivo, disponibilidade e apoio que sempre demonstrou, aqui lhe exprimo a minha gratidão.

Ao Doutor João Tomé pela coorientação, disponibilidade e ajuda para a realização deste trabalho. Desejo-lhe muito sucesso.

À Beatriz Martins, a minha profunda gratidão por toda a ajuda e disponibilidade, por ter-me ensinado tudo o que precisava de saber no laboratório, pela paciência e amizade.

Às minhas colegas Andreia Melo e Madania Amorim pela amizade, incentivo e ajuda no decorrer deste ano.

A todas as pessoas do iCBR que me ajudaram ao longo deste ano, pela disponibilidade e apoio proporcionados, que possibilitou a elaboração desde trabalho.

À minha família, pai, mãe e irmã, em especial, pelo apoio incondicional e palavras de incentivo. Foram vocês que estiveram lá nos bons e maus momentos. Sem vocês não teria esta oportunidade de seguir o meu sonho e objetivos.

Aos meus amigos e colegas pela paciência, atenção e força que prestaram em momentos mais difíceis, o meu maior obrigado.

E um obrigado a todas as pessoas com que me fui encontrando, que de alguma forma foram dando forças para continuar.

# Table of Contents

List of Figures ............ xiii

List of Tables ............ xv

Abbreviations ............ xvii

Abstract ............ xix

Resumo ............ xxi

Chapter 1 – Introduction and Aims ............ 1

1.1 Age-related Macular Degeneration ............ 3

1.1.1 Prevalence, classification and diagnosis ............ 3

1.1.2 Pathogenesis ............ 4

1.1.3 Dry and wet forms of AMD ............ 5

1.1.4 Treatment of AMD ............ 7

1.2 Extracellular Vesicles (EVs) ............ 8

1.2.1 Biogenesis and release of extracellular vesicles ............ 8

1.2.2 Extracellular Vesicles as drug delivery systems ............ 10

1.3 Photodynamic Therapy (PDT) ............ 13

1.3.1 Brief history and applications of PDT ............ 13

1.3.2 Components and mechanism of action of PDT ............ 14

1.3.3 Photosensitizers ............ 16

1.3.4 Light source ............ 18

1.3.5 Mechanisms of cell death ............ 18

1.3.6 Photodynamic Therapy in Age-related Macular Degeneration: State-of-art ............ 19

1.4 Aims of the study ............ 20

Chapter 2 – Materials and methods ............ 23

2.1 Preparation of $ZnTPPF_{16}(SGal)_4$ working solution ............ 25

2.2 Photosensitizer absorbance ............ 25

2.3 Maintenance of ARPE-19 cell line ............ 25

**2.4 Isolation of exosomes** .......... 27

**2.4.1 Isolation of ARPE-19 cell-derived exosomes** .......... 27

**2.4.2 Isolation and purification of RPE cell-derived exosomes from porcine eyecups** .......... 27

**2.5 Exosome loading with ZnTPPF$_{16}$(SGal)$_4$** .......... 28

**2.6 Determination of fluorescence and absorbance of the exosomal ZnTPPF$_{16}$(SGal)$_4$** .......... 28

**2.7 Determination of total protein concentration** .......... 28

**2.8 Treatment of ARPE-19 cells with ZnTPPF$_{16}$(SGal)$_4$ and exosomal ZnTPPF$_{16}$(SGal)$_4$** .......... 29

**2.9 Determination of intracellular photosensitizer concentration by fluorimetry** .......... 29

**2.10 Photodynamic assays** .......... 30

**2.11 MTT colorimetric assay** .......... 31

**2.12 Western Blotting** .......... 31

**2.13 Nanoparticle Tracking Analysis (NTA)** .......... 33

**2.14 Transmission Electron Microscopy (TEM)** .......... 33

**Chapter 3 – Results** .......... 35

**3.1 Photophysical properties of ZnTPPF$_{16}$(SGal)$_4$** .......... 37

**3.2 Characterization of RPE-derived exosomes** .......... 37

**3.3 Incorporation of ZnTPPF$_{16}$(SGal)$_4$ into exosomes** .......... 38

**3.4 Cellular uptake of ZnTPPF$_{16}$(SGal)$_4$ in ARPE-19 cells** .......... 41

**3.5 ZnTPPF$_{16}$(SGal)$_4$ induces phototoxicity in ARPE-19 cells** .......... 42

**3.6 Exosomal ZnTPPF$_{16}$(SGal)$_4$ induces phototoxicity in ARPE-19 cells** .......... 43

**Chapter 4 – Discussion** .......... 45

**Chapter 5 – Conclusion** .......... 51

**Bibliography** .......... 55

# List of Figures

Figure 1. Visual field through a healthy eye (left) and the eye on AMD patient (right) ... 3

Figure 2. Diagrams illustrating the anatomical changes in a human retina experiencing dry and wet AMD ... 6

Figure 3. Scheme of biogenesis of EVs and components of exosomes ... 9

Figure 4. Schematic representation of organs targeted by EVs-contained drugs. ... 12

Figure 5. Timeline of PDT development ... 14

Figure 6. Mechanism of action of photodynamic therapy (A) and photochemical kinetics of PDT (Jablonski diagram) showing type-I and type-II processes (B). ... 15

Figure 7. Chemical structure of a porphyrin with a zinc metal atom in the core, conjugated with four molecules of galactose, $ZnTPPF_{16}(SGal)_4$. ... 20

Figure 8. Representative images of the LED array system. ... 30

Figure 9. Electronic absorption spectrum of $ZnTPPF_{16}(SGal)_4$ at 2, 20 and 50 μM in DMSO and in PBS with 0.5% DMSO. ... 37

Figure 10. Characterization of exosomes isolated from ARPE-19 cells and porcine eyecups ... 38

Figure 11. Calibration curve of fluorescence intensity versus concentration of $ZnTPPF_{16}(SGal)_4$ from 0 to 60 μM ... 39

Figure 12. Absorbance of $ZnTPPF_{16}(SGal)_4$ encapsulation ... 40

Figure 13. Transmission electron microscopy (TEM) of exosomes (A) and exosomal $ZnTPPF_{16}(SGal)_4$ ... 41

Figure 14. Intracellular uptake of $ZnTPPF_{16}(SGal)_4$ by ARPE-19 cells. ... 41

Figure 15. Toxicity of $ZnTPPF_{16}(SGal)_4$ in ARPE-19 cells in dark conditions (A) and after light irradiation (B). ... 42

Figure 16. Exosomal $ZnTPPF_{16}(SGal)_4$ is nontoxic in darkness (A) and induces phototoxicity in ARPE-19 cells (B). ... 44

# List of Tables

**Table 1. List of the most relevant approved photosensitizers for PDT................. 17**
**Table 2. Primary Antibodies used in Western Blot assay...................................... 32**
**Table 3. ZnTPPF$_{16}$(SGal)$_4$ fluorescence intensity before and after purification ... 39**
**Table 4. ZnTPPF$_{16}$(SGal)$_4$ encapsulation efficiency ................................................ 40**
**Table 5. Amount of exosomal ZnTPPF$_{16}$(SGal)$_4$ and corresponding ZnTPPF$_{16}$(SGal)$_4$ concentrations.................................................................. 43**
**Table 6. ZnTPPF$_{16}$(SGal)$_4$ concentration and respective quantity of ZnTPPF$_{16}$(SGal)$_4$................................................................................................ 43**

# Abbreviations

AMD – Age-related Macular Degeneration
BCA – Bicinchoninic Acid Assay
BSA – Bovine Serum Albumin
CNV – Choroidal Neovascularization
DMSO – Dimethyl sulfoxide
ECM – Extracellular matrix
EMT – Epithelial-mesenchymal transition
ESCRT – Endosomal sorting complex required for transport
EV – Extracellular Vesicle
Exo – Exosome
FDA – Food and Drug Administration
GA – Geographic Atrophy
Hp – Hematoporphyrin
HpD – Hematoporphyrin derivative
ILV – Intraluminal Vesicle
LDL – Low-density lipoprotein
MTT – 3-(4,5-dimethylthiazol-2-yl)-2,5-diphenyltetrazolium bromide
MVB – Multivesicular Bodies
MVE – Multivesicular endosome
NTA – Nanoparticle Tracking Analysis
PBS – Phosphate Buffered Saline
PDT – Photodynamic Therapy
PVDF – Polyvinylidene Difluoride
PS – Photosensitizer
ROS – Reactive Oxygen Species
RPE – Retinal Pigment Epithelial
SDS – Sodium Dodecyl Sulfate
TEM – Transmission Electron Microscopy
VEGF – Vascular endothelial growth factor

# Abstract

Age-related macular degeneration (AMD) is a progressive, chronic disease that affects individuals over 50 years and induces loss of central vision. Early stages of AMD are not usually associated with declined in visual acuity. However, the disease can progress from early to advanced forms, dry and wet AMD, in which geographic atrophy of the retinal pigment epithelium and choroidal neovascularization occur, respectively. In some cases, RPE detachment and subretinal fibrosis are also present in advanced forms of AMD. Although administration of intravitreal injections with anti-VEGF (vascular endothelial growth factor) drugs can stop the formation of new vessels from choroid or improve temporarily the visual acuity, there are some individuals that do not respond to the treatment. Moreover, this kind of treatment can increase fibrosis in CNV.

In some cases, photodynamic therapy (PDT) is used in combination with anti-VEGF therapy. PDT is based on three non-toxic components *per se*: photosensitizer (PS), light with the appropriate wavelength and oxygen. In the treatment of neovascular form of AMD by PDT, a photosensitizer is administered intravenously and accumulated in the CNV. When the eye is exposed to an appropriate wavelength of light, this PS generates reactive oxygen species (ROS) resulting in CNV vaso-occlusion and consequent death of abnormal vessels from choroid. However, currently there is no therapy to subretinal fibrosis. Galectins are a family of proteins that play an important role both in CNV and subretinal fibrosis in AMD.

The main purpose of this study was to investigate whether a based exosome-porphyrin nanoformulation is able to enhance AMD PDT efficacy. In this work, a PS-carbohydrate conjugate, $ZnTPPF_{16}(SGal)_4$, which could be recognized by galectin-1, which is overexpressed in advanced AMD. We characterized the exosomes isolated from conditioned media of ARPE -19 cell line and porcine eyecups, using Western Blot and NTA techniques. For the encapsulation of the photosensitizer, we used exosomes isolated from the retinal pigment epithelium of porcine eyecups. Exosomal $ZnTPPF_{16}(SGal)_4$ have been purified and characterized in photophysical terms, namely by absorbance and fluorescence studies due to the optic properties of our compound. Transmission electron microscopy analysis has suggested $ZnTPPF_{16}(SGal)_4$ was encapsulated in exosomes. Biological studies of the free $ZnTPPF_{16}(SGal)_4$ *vs* exosomal $ZnTPPF_{16}(SGal)_4$ were performed on an ARPE-19 cell line (with morphology reminiscent of fibroblasts). It was found that $ZnTPPF_{16}(SGal)_4$ was internalized by ARPE-19 cells. Both $ZnTPPF_{16}(SGal)_4$ and exosomal $ZnTPPF_{16}(SGal)_4$ were non-toxic until activation by light. $ZnTPPF_{16}(SGal)_4$ demonstrated high efficacy in inducing ARPE-19 cell death

after photoactivation. However, the exosomal $ZnTPPF_{16}(SGal)_4$ did not enhance PDT. Further detailed studies with alternative methods that offer more efficient encapsulation of $ZnTPPF_{16}(SGal)_4$ in cell-derived exosomes, as well as further investigation towards therapeutic efficacy for sub-retinal fibrosis and CNV in AMD, are required.

# Resumo

A degenerescência macular da idade (DMI) é uma doença crónica e progressiva, caraterizada por perda da visão central, em indivíduos acima dos 50 anos de idade. Nas fases iniciais, a DMI é geralmente assintomática, não estando associada à diminuição da acuidade visual. No entanto, a doença pode progredir para formas mais avançadas, como a forma não exsudativa e a forma neovascular, que se manifestam por atrofia geográfica e a neovascularização coroideia, respetivamente. Em alguns casos, o descolamento do epitélio pigmentado da retina e a fibrose sub-retiniana também se encontram presentes nas formas avançadas da DMI. Apesar da administração de injeções intravítreas de agentes anti-VEGF (fator de crescimento endotelial vascular) poder inibir a formação de novos vasos da coróide e permitir uma melhoria da acuidade visual, esta é temporária e, por outro lado, existem alguns doentes que não respondem ao tratamento. Além disso, este tipo de tratamento pode aumentar a fibrose na neovascularização da coróide (CNV). Em alguns casos, a terapia fotodinâmica (PDT) é utilizada em combinação com a terapia anti-VEGF. A PDT combina três componentes não tóxicos individualmente: fotossensibilizador (PS), luz com comprimento de onda apropriado e oxigénio molecular. O tratamento da forma exsudativa da DMI com PDT envolve a administração de um fotossensibilizador (PS) por via intravenosa. Após acumulação na retina, o PS é ativado com luz de comprimento de onda apropriado. Quando fotoativado, o PS gera espécies reativas de oxigénio (ROS) que promovem a oclusão da membrana neovascular, havendo destruição dos neovasos da coróide. No entanto, a PDT no tratamento da DMI tem caído em desuso desde o aparecimento dos anti-VEGF. As galectinas são uma família de proteínas que têm uma função importante no desenvolvimento da CNV e fibrose sub-retiniana na DMI.

O principal objetivo deste estudo foi investigar de que forma uma nanoformulação de exossomas com uma porfirina é capaz de potenciar a eficácia da PDT na DMI. Neste estudo, utilizou-se um PS galacto-conjugado ($ZnTPPF_{16}(SGal)_4$), que poderá eventualmente ser reconhecido pela galectina-1, que se encontra sobre-expressa nos estádios mais avançados da DMI.

Os exossomas isolados do meio condicionado de células ARPE-19 e de *eyecups* de suínos, foram caraterizados por Western Blotting e análise de rastreamento de nanopartículas (NTA).

O complexo exossoma-$ZnTPPF_{16}(SGal)_4$ foi caraterizado em termos fotofísicos, nomeadamente por estudos de absorvência e de fluorescência devido às propriedades óticas do nosso composto. Resultados de microscopia eletrónica de transmissão sugeriram que o $ZnTPPF_{16}(SGal)_4$ foi encapsulado em exossomas. Foram realizados estudos *in vitro* com $ZnTPPF_{16}(SGal)_4$ livre *vs* $ZnTPPF_{16}(SGal)_4$ exossomal utilizando a linha celular ARPE-19 (com morfologia reminiscente de fibroblastos) de forma a avaliar a captação dos mesmos pelas células e a citotoxidade no escuro e após irradiação com luz. O $ZnTPPF_{16}(SGal)_4$ foi captado pelas células ARPE-19. Tanto o $ZnTPPF_{16}(SGal)_4$ livre como o $ZnTPPF_{16}(SGal)_4$ exossomal não são tóxicos no escuro. Após fotoativação, ambos são eficazes na indução de morte das células ARPE-19. No entanto, $ZnTPPF_{16}(SGal)_4$ exossomal não potenciou o efeito fotodinâmico. Serão necessários estudos mais detalhados, com métodos alternativos que permitam um encapsulamento mais eficiente do $ZnTPPF_{16}(SGal)_4$ em exossomas, assim como, investigação adicional da sua eficácia terapêutica para a fibrose sub-retiniana e CNV na DMI.

# Chapter 1 –

# Introduction and Aims

## 1.1 Age-related Macular Degeneration

### 1.1.1 Prevalence, classification and diagnosis

Age-related macular degeneration (AMD) is an eye disease that causes macular degeneration with central vision loss. It is a leading cause of irreversible blindness and visual impairment in patients over 60 years old (Fig. 1). Estimates indicate that more than 196 million people worldwide have AMD and this number is expected to increase to 288 million by 2040[1].

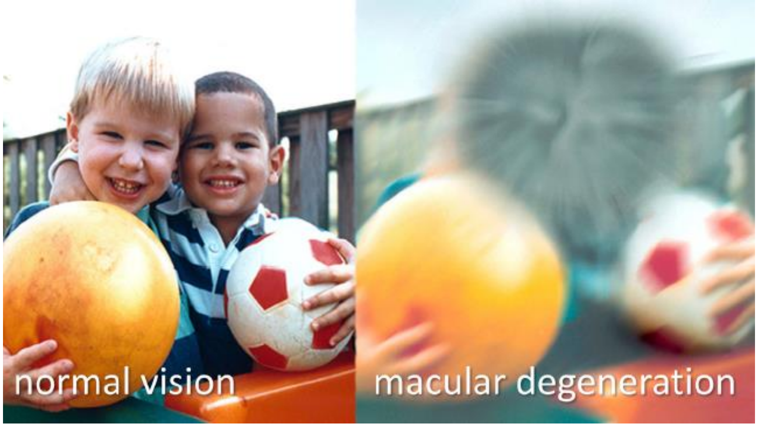

**Figure 1**. **Visual field through a healthy eye (left) and the eye on AMD patient (right)**. (Adapted from Ljubimov, 2017[2])

AMD incidence is higher in women than in men in all age groups[3]. A global meta-analysis showed that in white European people the prevalence of early and late AMD is twice as much compared with Asian people. The prevalence of AMD is also higher in white Europeans in comparison with African people. The prevalence of neovascular AMD is similar in all ethnic groups[1]. AMD risk is also influenced by non-genetic and environmental factors, such as smoking and diet. Other factors with less evidence are sunlight exposure, iris colour and alcohol consumption[4,5]. However, aging is a major risk factor for AMD, and it is associated with biological changes in the eye and with cumulative oxidative injury[6]. AMD is characterized by the presence of drusen (extracellular deposits) in the macula (pigmented area near the center of the retina), thickening of the Bruch's membrane and gradual death of retinal pigment epithelial cells and photoreceptors. As RPE cells and photoreceptors degenerate, there is a propensity for the growth of blood vessels away from their normal location in the choroid into an abnormal location beneath the retina. These abnormal blood vessels are dysfunctional and leaky, resulting in progressive and severe loss of the central vision[7].

AMD can be classified as early AMD and late AMD. Early AMD is usually asymptomatic, with some patients noticing mild central distortion. In late AMD central vision is affected. Advanced AMD has two forms, geographic atrophy (GA) and choroidal neovascularization (CNV). In the former, the progression of the disease is relatively slow, but in the latter it can progress rapidly[8]. The earliest symptoms of late AMD include distorted vision when reading, driving or watching television, and a dark patch in the central vision, resulting in a difficulty in face recognition. The presence of fluid or retinal hemorrhage, retinal epithelial detachments, hard exudate or subretinal fibrous scar tissue are typical lesions in neovascular AMD. Atrophic AMD or GA are characterized by an outer retinal thinning. Atrophic AMD can be unifocal or multifocal and can surround but spare the central macula[9].

The diagnosis of AMD is based on clinical examination or assessment of colour fundus photographs[10]. In the last years, spectral-domain optical coherence tomography (SD-OCT) and fundus autofluorescence imaging have been used to detect lesions[11]. Fluorescein angiography is used to detect CNV and its location and activity. Optical coherence tomography angiography is a non-invasive approach that does need dye. This method detects the presence of choroidal vascular networks but does not detect leakage[9].

### 1.1.2 Pathogenesis

AMD has a complex multifactorial aetiology. Although changes are found in several ocular structures, such as photoreceptors, RPE, Bruch’s membrane and choriocapillaries, it seems that RPE dysfunction plays a pivotal role in AMD pathobiology[12]. RPE cells lying in direct contact with the outer segments of the photoreceptors are essential for the maintenance of their function and survival. RPE cells are involved in the absorption of scattered light, transport of metabolites and nutrients between photoreceptors and choriocapillaris, secretion of growth factors for photoreceptors and they are also responsible for phagocytizing shed photoreceptor outer segments[7].

In AMD, oxidative stress results in RPE and choriocapillaris injury[6]. RPE injury evokes a chronic inflammatory response in Bruch's membrane and choroid. In AMD eyes, RPE injury and inflammation stimulate the production and deposition of abnormal extracellular matrix (ECM) components derived not only from the RPE and photoreceptors cells but also from the systemic circulation. The abnormal ECM can cause further damage to the retina, RPE and choroid. Oxidative damage to the choriocapillaris contributes to the pathogenesis of AMD. The development of GA and growth of new vessels from the choroidal involve the perturbation of RPE-choriocapillaris homeostasis[6].

The formation of new blood vessels (angiogenesis), is a process that occurs when the endothelial cells of a mature blood vessel wall are activated by angiogenic factors like the vascular endothelial growth factor (VEGF) and fibroblast growth factor[13]. The activation promotes endothelial cell detachment from their basement membrane and other supporting peri-endothelial cells, allowing them to migrate, proliferate and form a capillary lumen. Angiogenesis is mostly mediated by VEGF receptors and integrins, but recent studies have shown that members of the galectin class of β-galactoside-binding proteins have the potential to modulate angiogenesis[14]. Galectin-3, a member of the galectin family of mammalian lectins, has been shown to promote corneal neovascularization[15] and galectin-1 to promote CNV-mediated subretinal fibrosis[16].

### 1.1.3 Dry and wet forms of AMD

AMD can be divided into several categories (Fig. 2). Early and intermediate AMD are characterized by the presence of drusen between the retinal pigment epithelium and Bruch’s membrane. Many patients with intermediate AMD eventually progress to the advanced stage of the disease. Advanced AMD includes GA and neovascular AMD. Early and intermediate AMD, along with GA, are referred as dry AMD, neovascular AMD is also referred as wet AMD.

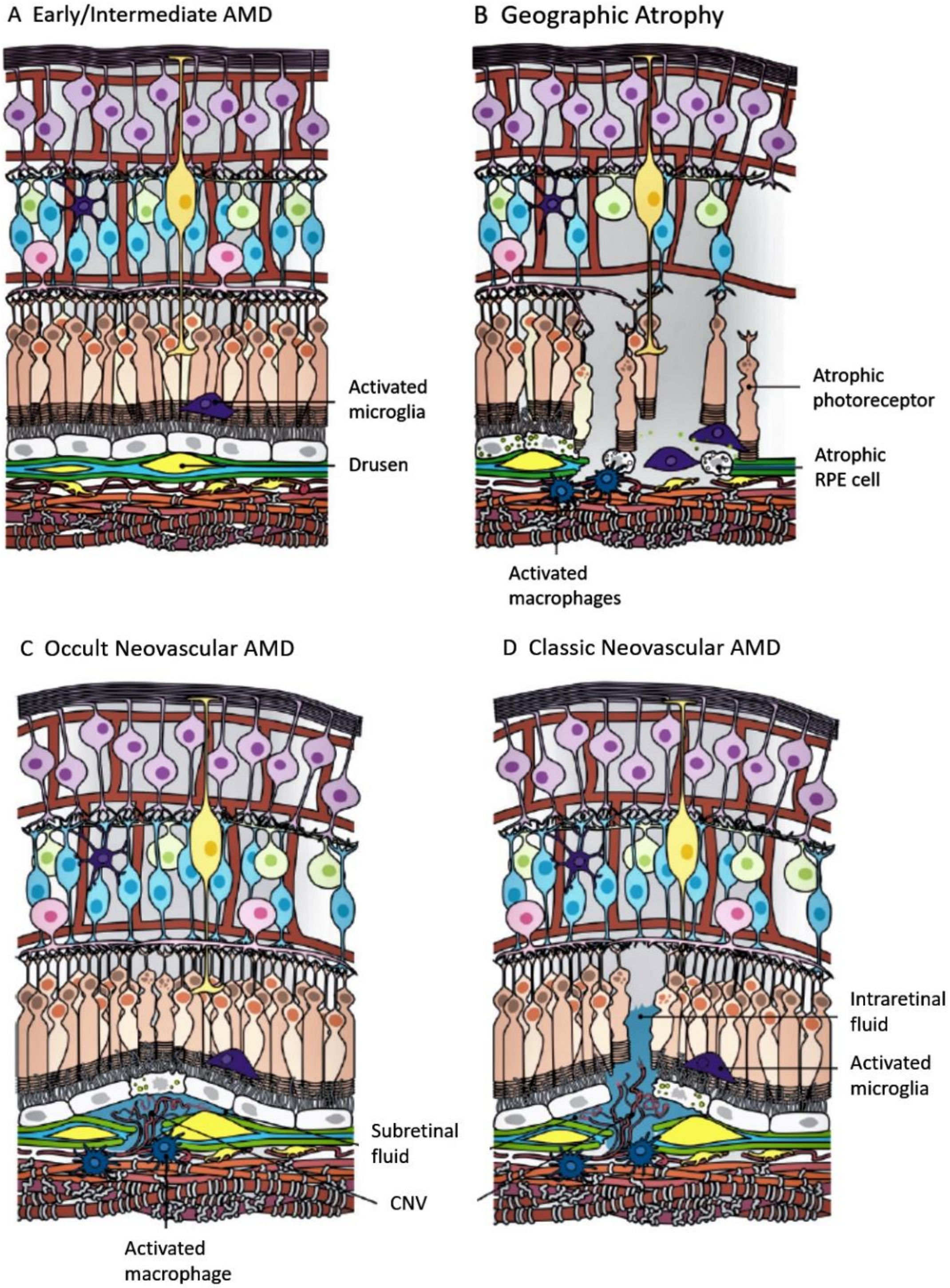
A Early/Intermediate AMD
B Geographic Atrophy
Activated microglia
Drusen
Atrophic photoreceptor
Atrophic RPE cell
Activated macrophages
C Occult Neovascular AMD
D Classic Neovascular AMD
Intraretinal fluid
Activated microglia
Subretinal fluid
CNV
Activated macrophage

**Figure 2. Diagrams illustrating the anatomical changes in a human retina experiencing dry and wet AMD:** (A) early/intermediate AMD characterized by the presence of drusen and (B) geographic atrophy, referred as dry AMD, representing a photoreceptor and RPE cell atrophy. (C) Occult and (D) classic neovascular AMD, also referred as wet AMD where Bruch's membrane is disrupted by neovessels. (Adapted from Van Lookeren Campagne, Lecouter, Yaspan, & Ye, 2014[17]).

The accumulation of lipid and protein wastes (drusen) induce structural and functional changes in Bruch's membrane and RPE. In fact, there is Bruch's membrane damage, loss of RPE barrier function and reduction of RPE ability to transport metabolic waste across Bruch's membrane. The choriocapillaris is less dense in patients with this form of AMD. Inflammation in the outer retina is noticeable by the presence of activated microglia cells. In GA, Bruch's membrane is severely disrupted. Atrophy and loss of both RPE and photoreceptor cells are noticeable. The choriocapillaris is perfused and inflammation is evident as activated microglia and macrophages are abundant in the degenerated area[17].

In occult neovascular AMD, the Bruch's membrane is disturbed by neovessels growing out from choriocapillaris. The leaky neovessels release fluid that accumulates under the RPE, distorting the local structure and causing stress in the RPE and photoreceptors cells. In a classic neovascular AMD, choroidal neovessels grow through the Bruch's membrane towards the RPE, penetrating through the RPE layer and advance into the photoreceptor layer resulting in intraretinal fluid accumulation in addition to subretinal fluid[17].

Both chronic damage of RPE and pre-existing neovascular lesions increase the risk of macular fibrosis. RPE cells can undergo epithelial-mesenchymal-transition (EMT). The same can occur with active vascular endothelial cells in CNV, which undergo endothelial-mesenchymal-transition (EndoMT)[18].

### 1.1.4 Treatment of AMD

Although there is no cure for AMD, there are some treatments for the wet form of the disease, such as anti-angiogenic drugs, laser therapy and photodynamic therapy (PDT). Anti-angiogenic agents are used with the main purpose to stop the formation of new blood vessels. The VEGF-A is an angiogenic factor that belongs to the VEGF family of growth factors[19]. It is a key regulator in the development of normal blood vessels and in the development of vessels in pathological conditions, such as AMD. Therefore, pharmacological approaches for neovascular AMD have been based on the inhibition of the angiogenic protein VEGF. The first anti-VEGF drug used in trials was pegaptanib sodium (Macugen®), an aptamer that binds VEGF165 and larger isoforms [9]. The second anti-VEGF drug approved by the US Food and Drug Administration (FDA) was ranibizumab, an antibody fragment that binds all VEGF isoforms. Other anti-VEGF drugs approved are bevacizumab (Avastin™) and aflibercept (Eylea®). Two major issues exist in the use of anti-VEGF drugs. The first is the need for a strict dosing regimen and the second is related to safety. Both ranibizumab (Lucentis®) and bevacizumab enter the systemic circulation substantially after intravitreal administration. Laser photocoagulation of the choroidal neovascular membranes has performed to prevent severe vision loss in patients with wet AMD, but this method is associated with high recurrence rates and can induce vision loss, principally when used to treat subfoveal choroidal neovascular membranes[20].

PDT with verteporfin was introduced in the late 1990s and consists of an intravenous infusion of the green photosensitizing dye, which is preferentially accumulated in neovascular membranes, followed by dye activation with light in a specific wavelength. This results in the generation of reactive oxygen species that damage the endothelium, promoting closure of new vessels. This photosensitizer specifically targets choroidal neovessels, which retains the dye more avidly than normal vessels, allows a directed targeting in the lesion without damaging surrounding tissues [21,22]. However, several side effects have been reported during and after PDT, including secondary subretinal hemorrhage, retinal pigmented epithelium tears and choroidal ischemia[23]. After PDT, patients need to avoid sun exposure and other sources of bright light.

## 1.2 Extracellular Vesicles (EVs)

### 1.2.1 Biogenesis and release of extracellular vesicles

Extracellular vesicles (EVs) are cell-derived membranous structures. They are divided into three subpopulations: exosomes, microvesicles and apoptotic bodies[24].

Exosomes were first observed by Pan and Johnstone when they were studying the maturation process of reticulocytes to erythrocytes, in 1983. At first, it was believed that the only function of exosomes was as cellular garbage disposal. Subsequent studies have shown that exosomes have an important role in intercellular communication and other important roles in biological processes[25].

Exosomes are derived from the endosomal compartments, named multivesicular bodies (MVB) and have a diameter in the range of 30 to 150 nm[26]. Previous reports have reported that EVs carry functionally active biological material, such as proteins, mRNAs and miRNAs[27]. This results in the capacity of transmitting signals to target cells in the surrounding environment and to distant organs, via blood and lymphatic vessels[28]. Recent research has also shown that mitochondrial DNA and chromosomal DNA are present inside exosomes[29]. The content of exosomes depends on their cell origin and microenvironment[30].

Exosomes have in their composition membrane-bound tetraspanins (CD9, CD63, CD81), lysosomal proteins (LAMP2B), fusion proteins (GTPase, Annexin), heat shock proteins (HSC70) and proteins involved in the biogenesis of MVBs (TSG101)[30]. Previous studies have shown that tetraspanins have a role in signal transduction, regulation of cell morphology, activation, invasion, fusion, motility, cell development and growth and cell adhesion[31]. Other proteins responsible for EVs uptake are integrins, that are involved in adhesion, proteoglycans or lectins[32].

Exosomes are present in cells from the retinal pigment epithelium and in drusen, a precursor of wet CNV, in patients with AMD, and some reports have shown that exosomes derived from RPE cells play part in neovascularization[33].

EVs have been isolated from cell lines and biofluids, such as blood, urine, tear, saliva, nasal secretions, semen and cerebrospinal fluid[32]. The most common method for isolation of EVs is ultracentrifugation, where a first centrifugation removes large cellular debris followed by ultracentrifugation (at 100000 x *g*)[34]. Other methods include purification by density gradient and use of serial filtration. In recent times, new methods claiming fast and simple exosome-purification are commercially available[35] .The purity is confirmed using electron microscopy and performing Western Blotting[36,37].

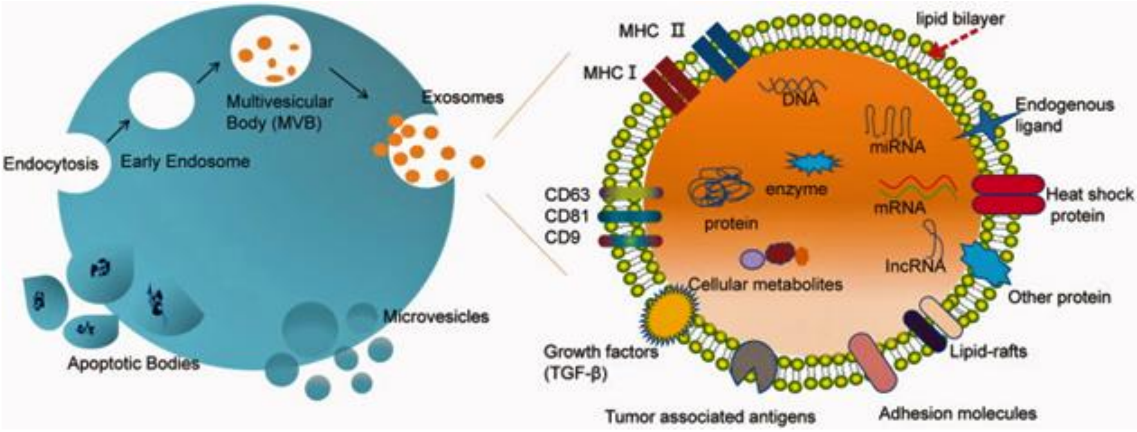
Endocytosis
Early Endosome
Multivesicular Body (MVB)
Exosomes
Apoptotic Bodies
Microvesicles
MHC II
MHC I
lipid bilayer
DNA
miRNA
Endogenous ligand
CD63
CD81
CD9
enzyme
protein
mRNA
Heat shock protein
lncRNA
Cellular metabolites
Other protein
Growth factors (TGF-β)
Lipid-rafts
Tumor associated antigens
Adhesion molecules

**Figure 3. Scheme of biogenesis of EVs and components of exosomes.** The exosome surface is decorated with various membrane proteins responsible for different pathophysiological functions. (Adapted from Meng et al., 2020[38])

Exosomes, a subtype of EVs, are released from cells as a result of the fusion of multivesicular endosome (MVE) with plasma membrane[39]. As the early endosomes mature into late endosomes, they accumulate intraluminal vesicles (ILV) within their lumen, originating MVB (Fig. 3). In most cells, MVB are going to fuse with lysosomes, resulting in the destruction of their content, but if the organelles contain hallmarks of

MVB, they can fuse with the plasma membrane, resulting in the release of their content into the extracellular milieu[40].

Endosomes can be divided into three compartments: early endosomes, late endosomes and recycling endosomes. Early endosomes result from the fusion with endocytic vesicles. The late endosomes are targeted to fuse with lysosomes or the plasma membrane. When the fusion with a lysosome occurs, it will result in the destruction of the content of the late endosome, but if the fusion of the late endosome/MVB is with the plasma membrane it results in the secretion of small vesicles, exosomes[36].

Previous studies revealed two distinct processes in the ILV formation. The first process is the result of the organization of the endosome membrane into units that are enriched with tetraspanins, a class of membrane proteins, that consist of four transmembrane domains that create a tertiary structure. The tetraspanins enriched microdomains, are thought to cluster proteins that are required for ILV formation through protein-protein interactions. CD9 and CD63 are two tetraspanins that are thought to play an import role in exosome formation and are frequently used to identify exosomes. The second process involves a series of complexes, the endosomal sorting complex required for transport (ESCRT)[21], consisting of four multi-protein complexes (ESCRT-0, -I, -II, -III). After the recognition and binding, EVs can be internalized into endosomal compartment of a recipient cell, via receptor-mediated endocytosis. This process is an energy-requiring process. EVs with a higher diameter are internalized by phagocytosis, and small EVs are taken up by other processes[32].

### 1.2.2 Extracellular Vesicles as drug delivery systems

In recent years, there has been an increase in the interest of EVs as potential drug delivery vehicles, since EVs have significant advantages over other drug delivery systems, such as liposomes and polymeric nanoparticles. Some of the advantages of EVs are the fact that they are obtained from patient's cells or blood, so they do not invoke the immune system as synthetic formulations do. Another advantage is the fact that EVs can directly fuse with the targeted plasma membrane, resulting in a more efficient internalization of the encapsulated drugs, and this is because EVs have a phospholipid bilayer[28]. They also avoid phagocytosis by monocytes and macrophages of the reticuloendothelial system due to its hydrophilic shell and anti-phagocytosis surface markers[41].

Liposomes are commonly used as nano-based drug delivery vehicle because of their non-toxicity and because of their size, they can accommodate a higher load of drugs, yet an inadequate *in vivo* targeting efficiency and a potential immunogenicity as limited their used in therapeutics. EVs have a membrane characterized by the presence of proteins for active targeting, adhesion, cell fusion and intracellular release of their content, making the EVs an ideal vehicle for drug delivery[28].

The drug loading methodologies for exosome-based drug delivery are divided into two groups: pre-loading and post-loading. In pre-loading methods, the drug is loaded in the parental cells, so, the EVs isolated or produced by them are already pre-loaded with the drug. In post-loading methods, the drug is encapsulated in the EVs after their isolation[42]. To encapsulate cargo into exosomes, several methods have been reported including incubation by simple incubation of the exosomes with the cargo, sonication, electroporation, extrusion, freeze/thaw cycle method and saponin-assisted loading[43]. Nonetheless, mechanical or physical insults can compromise the membrane integrity as well as protein integrity[44].

Water-insoluble chemicals can interact and cross the hydrophobic membrane of exosomes, increasing *in vivo* the drug bioavailability. Previous studies have shown that exosomes loaded with chemotherapeutics drugs show stronger cytotoxicity against drug-resistant cancer cell lines *in vitro* and stronger anti-tumor activity *in vivo* in comparison with free drugs[45].

Exogenous loading technique requires further purification of EVs in order to separate drug loaded EV from free drug and non-EV contaminants. The purification can be achieved by using techniques such as size-exclusion chromatography or filtration. Ultracentrifugation is the most used method to isolate EVs, but it is not recommended to purify EVs for therapeutic purposes because it might co-isolate protein aggregates. The presence of EV aggregates and contaminants in the isolated fraction is going to interfere with the quantification of EVs, leading to an underestimation or overestimation of the concentration of EVs[46].

It is not well known the mechanism by which exosomes from different cells transmit information to recipient cells. There are reports showing that exosomes affect the function of recipient cells by acting at the cell surface, transmitting information without release of their contents. On the other hand, exosomes are characterized by the enclosure and delivery of their content protected by the lipidic bilayer, so it is believed that exosomes are more prone to release their contents rather by acting at the cell surface after being captured by recipient cells[47]. Though EVs have the potential to be a drug delivery vehicle, there are some limitations, for example, EVs might be cleared rapidly from blood circulation[32].

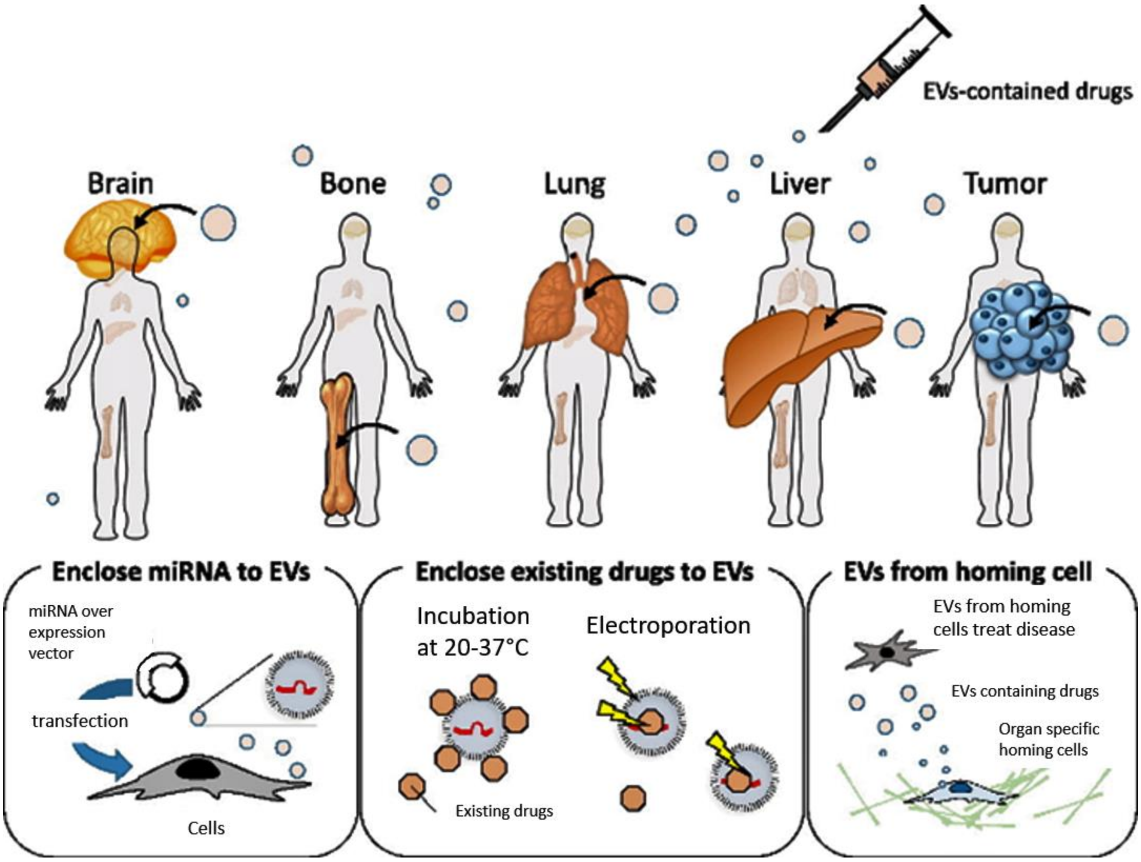
EVs-contained drugs
Brain
Bone
Lung
Liver
Tumor
Enclose miRNA to EVs
miRNA over expression vector
transfection
Cells
Enclose existing drugs to EVs
Incubation at 20-37°C
Electroporation
Existing drugs
EVs from homing cell
EVs from homing cells treat disease
EVs containing drugs
Organ specific homing cells

**Figure 4. Schematic representation of organs targeted by EVs-contained drugs.** Different approaches to enclose miRNA and drugs in EVs. (Adapted from Tominaga, Yoshioka, & Ochiya, 2015[48]).

Exosomes may deliver their cargo by rapid fusion with the target cell or receptor-mediated endocytosis. After reaching specific recipient cells, the exosomal surface molecules can bind membrane receptors. The exosomal content is then released into the cytoplasm, resulting in changes to the intracellular compartment of the recipient cell[49]. Secreted exosomes can be taken up by the target cells by three possible mechanisms: simple fusion through cellular membrane, endocytosis and activation of target cells[50].

Even though that some reports have shown that EVs accumulate in bone marrow, lungs, brain, lymph nodes and tumor tissue, there is not enough evidence supporting specific organ tropism (Fig. 4)[48].

Therefore, strategies of drug attachment or encapsulation into EVs, preservation of the EVs and establishment of organ tropism are important factors that must be considered when using EVs as a drug delivery system.

## 1.3 Photodynamic Therapy (PDT)

### 1.3.1 Brief history and applications of PDT

The treatment of diseases with the use of phototherapy can be traced back over 4000 years to the ancient Egyptians. Contemporary PDT stands first in the early twentieth century (Fig. 5)[51].

The first application of a photosensitizing agent in combination with light was reported by a medical student, Oscar Raab[52]. During his experiments with acridine dye, he noticed that fluorescence occurs in protozoa which had been treated with dyes and irradiated. This circumstance triggered the consumption of oxygen and the toxic effect, that lead to the death of the protozoa. Raab gave his observations to his professor, Professor Von Tappeiner, who described this phenomenon as a photodynamic effect, in 1904. A year later, in 1905, the first effective attempt of skin cancer treatment using an eosin solution was performed. Nonetheless, this therapy did not influence the scientific community and was forgotten for decades[53].

Figge reported in 1948, a recap of studies that showed that when porphyrins were exogenously administered, they were selectively accumulated in murine tumors. The study was then extended to include patients with cancer, where an injection of a crude preparation of hematoporphyrin led to selective tumor fluorescence[54]. Modern PDT was initiated with the discovery of cancer diagnostic and therapeutic effects of a hematoporphyrin derivative, in the 1960s[55,56]. After the first clinical approval in the 1990s, Photofrin has been clinically approved for PDT of several types of cancer [57]. Besides this therapeutic approach has been used for the treatment of many types of cancers, in some non-oncological disorders, in dermatological disorders and wet AMD, it has been also applied[51]. PDT has several advantages. It is a procedure that can be repeated multiple times because of the lack of cumulative toxic effects, works in certain types of diseases and due to its low-risk profile it can be used by the elderly or people not recommended for surgery. The main disadvantage is sensitization to light.

However, there are some limitations to PDT. The photosensitizer (PS) is injected into the bloodstream and is absorbed by cells of the entire body. It has been reported that PS remains in diseased cells for a longer period of time in comparison to healthy cells, so the light exposure needs to be carefully timed so it occurs when almost all PS is mainly present in unhealthy cells, and preferentially those are also being exposed to light. The efficacy of PDT depends on the yield of singlet oxygen produced in the diseased cells, which depends on the concentration of molecular oxygen in the tissue[58]. After the success of preclinical and clinical studies showing a good efficacy and safety of PDT with verteporfin for the treatment of CNV, this photosensitizer was approved by the FDA in 2000[59].

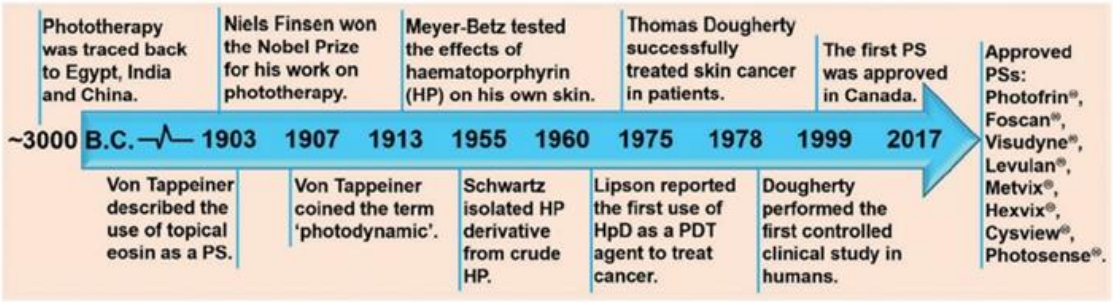
Phototherapy was traced back to Egypt, India and China.
Niels Finsen won the Nobel Prize for his work on phototherapy.
Meyer-Betz tested the effects of haematoporphyrin (HP) on his own skin.
Thomas Dougherty successfully treated skin cancer in patients.
The first PS was approved in Canada.
Approved PSs: Photofrin®, Foscan®, Visudyne®, Levulan®, Metvix®, Hexvix®, Cysview®, Photosense®.
~3000 B.C.
1903
1907
1913
1955
1960
1975
1978
1999
2017
Von Tappeiner described the use of topical eosin as a PS.
Von Tappeiner coined the term 'photodynamic'.
Schwartz isolated HP derivative from crude HP.
Lipson reported the first use of HpD as a PDT agent to treat cancer.
Dougherty performed the first controlled clinical study in humans.

**Figure 5. Timeline of PDT development.** (Adapted from Kim, Jo, & Na, 2020[59]).

### 1.3.2 Components and mechanism of action of PDT

The molecular mechanism of PDT is based on the combination of three components: photosensitizer, light with the appropriate wavelength, and molecular oxygen[60].

There are two mechanisms of photodynamic reaction. The first stage of the two mechanisms is similar (Fig. 6). A photosensitizer is irradiated with light at a specific wavelength coinciding with the PS absorption spectrum and is converted from the singlet energy state $S_0$ into the excited singlet state $S_1$, as a result of photon absorption. Some energy is radiated in form of a quantum of fluorescence and the remaining energy directs the PS molecule to the excited triplet state $T_1$, the therapeutic form of the compound[53].

In a biological medium, the reactive oxygen species (ROS) that are generated by the photodynamic process can react with proteins, nucleic acids and lipids. For example, the damage to these biomolecules may be irreversible in tumor cells resulting in necrosis, apoptosis or autophagy[61]. It can also cause tumor ischemia following PDT-induced vascular injury or activate the immune response against tumor antigens[62].

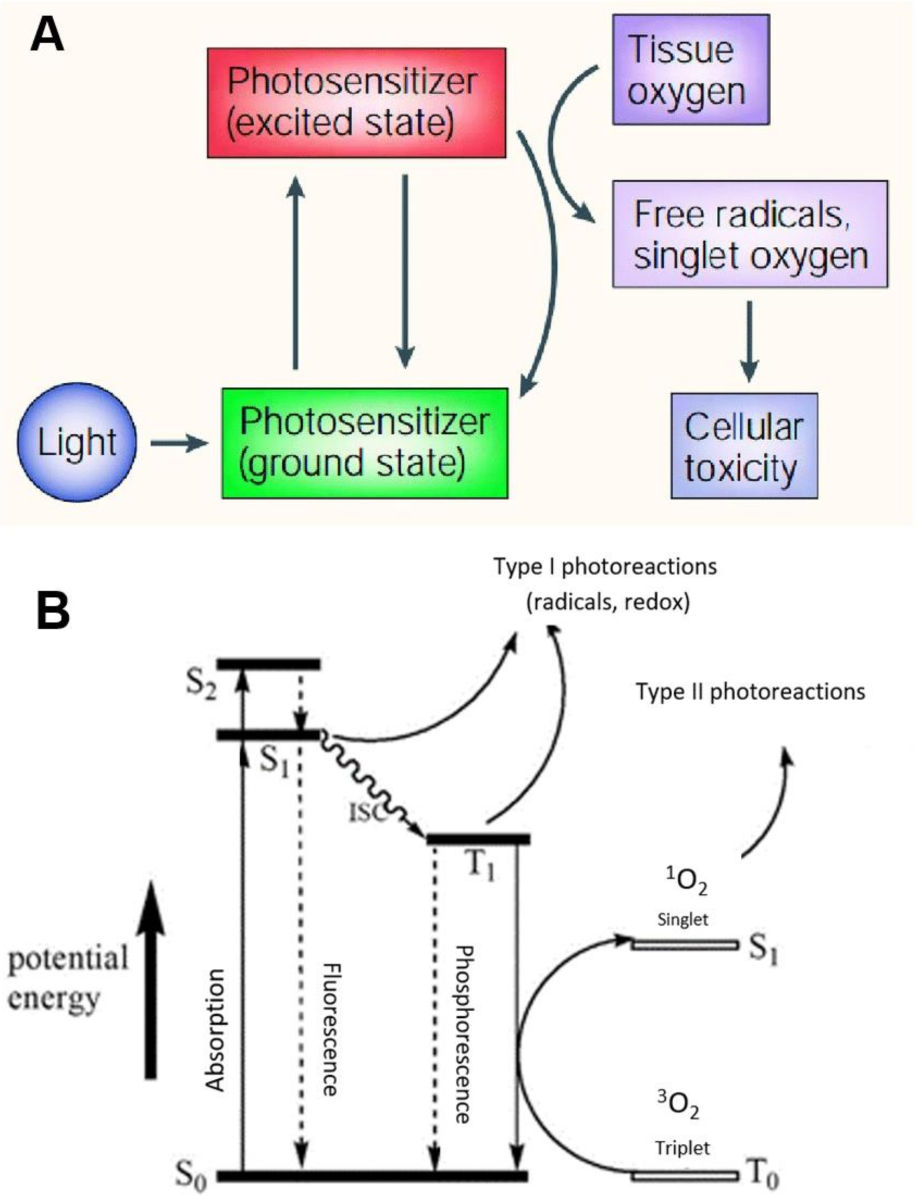
A
Photosensitizer (excited state)
Tissue oxygen
Free radicals, singlet oxygen
Light
Photosensitizer (ground state)
Cellular toxicity
B
Type I photoreactions (radicals, redox)
Type II photoreactions
S2
S1
ISC
T1
potential energy
Absorption
Fluorescence
Phosphorescence
1O2
Singlet
S1
3O2
Triplet
T0
S0

**Figure 6. Mechanism of action of photodynamic therapy (A) and photochemical kinetics of PDT (Jablonski diagram) showing type-I and type-II processes (B). (**Images adapted from Dolmans, Fukumura, & Jain, 2003[62] and Lin, Chen, & Liu, 2017[63]).

### *Type I mechanism of photodynamic reaction*

The production of superoxide anion by electron transfer from the triplet PS to molecular oxygen leads to the beginning of type I mechanism. When in the excited triplet state $T_1$, the PS can transfer a hydrogen or electron to biomolecules in its surrounding, leading to the formation of free radicals and anion radicals of the PS and the substrate. Electrons can also interact with oxygen molecules, that remain in their basic energetic state, but this process lead to the formation of radicals reactive oxygen species[53,64].

### *Type II mechanism of photodynamic reaction*

Energy of the PS in the excited triplet state is transferred directly to the oxygen molecule in the basic energetic state, to form molecular singlet oxygen. The direct transfer of energy between these two molecules is possible because they have the same spins[53].

Both type of ROS cause the photodamage of proteins, fats and other molecules in the photosensitized area[65]. This results in the direct death of target/unhealthy cells by apoptosis and/or necrosis processes. The damage of mitochondria can lead to apoptosis, and when there is a loss of structural integrity of the plasma membrane, cell undergoes necrosis. The damage of lysosomes or endoplasmic reticulum provokes autophagy[53].

Type I and type II reactions occur simultaneously, and the ratio between both depends on the type of PS used, the concentrations of substrate and oxygen and the binding ability of the sensitizer for the substrate. As a result of a high reactivity and a short half-life of the ROS, only the cells that are proximal to the area of the ROS production are affected by PDT[66].

The extent of photodamage and cytotoxicity depends on the type of photosensitizer, its extracellular or intracellular localization, the administered dose, the light exposure dose, oxygen availability and the time between administration of the drug and light exposure[62].

### 1.3.3 Photosensitizers

Photosensitizers are capable of absorbing light in a specific wavelength, triggering photochemical reactions and photophysical processes. An ideal PS needs to have the following characteristics: chemically pure or well characterized, quite photostable, high photochemical reactivity, low cytotoxicity in the dark, high selectivity for damaged tissue, simple synthesis/easily available and low price.

There are some important factors to be taken into consideration related to safety and efficacy of PDT. The maximum absorption of light should be between the wavelength of 600 and 900 nm. The absorbance bands should also not overlap the absorption band of other substances like melatonin or hemoglobin[53].

Porphyrins have been studied as photosensitizers in PDT in several cancers and AMD. Their planar aromatic structure, their photophysical properties and synthetic versatility has made them attractive agents for PDT[67]. In this context, several photosensitizers have been approved in clinical practice (Table 1).

**Table 1.** List of the most relevant approved photosensitizers for PDT

| | Name | Trademark | Manufacturer | Main applications |
|---|---|---|---|---|
| 1st Generation | Porfimer sodium | Photofrin® | Axcan Pharma, Canada | Esophageal cancer; Lung adenocarcinoma; Endobronchial cancer |
| 2nd Generation | Aminolevulinic acid hydrochloride | Ameluz® | DUSA, USA | Mild to moderate actinic keratosis |
| | Temoporfin | Foscan® | Biolitec, Germany | Head and Neck Neoplasms;<br>Carcinoma, Squamous Cell |
| | Talaporfin sodium | Laserphyrin® | Meiji Seika, Japan | Lung cancer,Malignant brain tumor |
| | Methyl aminolevulinate | Metvix® | Galderma, UK | Non-hyperkeratotic actinic kearatosis; Basal cell carcinoma |
| | Verteporfin | Visudyne® | Novartis, Switzerland | Age-related macular degeneration |

### First generation PS

The first PS was commercially available in the 1970s and it was introduced by Dr. Thomas Dougherty and his colleagues[68]. They were testing a water-soluble porphyrin mixture, a hematoporphyrin derivative (HpD), that was obtained by purification and chemical modification of the hematoporphyrin (Hp), a derivative of the blood protoporphyrin IX. This new modification showed better selectivity for tumors and less photosensitizing potential on the skin. The HpD with the monomeric porphyrins removed was approved by FDA and was available with the trade name of Photofrin[54]. This is one of the most used PS, however, the preparation has some limitations, such as low chemical purity and poor tissue penetration. Also, after PDT, due to its long half-life time and high accumulation in the skin results in skin hypersensitivity to light for several weeks[61]. The disadvantages of the first-generation photosensitizers lead to the development of new and improved compounds[53].

### Second generation PS

The second generation of PSs started in the 1980s. A considerable number of substances with potential photosensitizing properties has been proposed but only a few were used in clinical trials[53]. The second-generation PSs are composed of hematoporphyrin derivatives and synthetic PSs such as 5-aminolevulinic acid, benzoporphyrin derivatives, bacteriochlorin and phthalocyanines, among others[69]. This new generation of PSs is characterized by a light absorption at higher wavelengths, increasing the therapeutic window which allows a better penetration to deeply located tissues[33]. Plasma membrane, lysosomes, mitochondria and nuclei of tumor cells have been estimated to be potential PDT targets[70].

#### Third generation PS

Third generation PSs are based on the synthesis of substances with a higher affinity to tumor tissue, such as bioconjugates, reducing the surrounding damage of healthy tissue. In order to increase the selectivity of PSs, second generation PSs have been combined with molecules focused on the target receptor, such as: LDL lipoproteins, monoclonal antibodies, growth factor receptors, transferrin receptors or hormones. This results in an enhancement of the selectivity and a greater accumulation of the PS in affected areas[53].

### 1.3.4 Light source

PDT requires a precise dosimetry. The wavelength of the activating light determines the depth of light penetration into tissues. This is determined by the absorption spectrum of the PS used. The phototherapeutic window is generally between 600-900 nm. At the level of the retina, RPE and choroid, the increase in the absorption of light by melanin, macular lutein and hemoglobin in a lower wavelength range might decrease light penetration[71].

Several light sources can be used to activate the PS, but lasers are the standard light source for PDT due to several advantages[72]. Lasers can produce a monochromatic light beam with high intensities, are easy to control, can be focused to a small spot and can be transmitted by optical fibers, providing a precise light delivery to the treatment area.

For PDT it is crucial that the light distribution be uniform to obtain homogeneous phototoxicity. There is a variety of lasers available, but diode lasers are becoming the light source of choice because of their portability, size and because they are relatively inexpensive[71].

### 1.3.5 Mechanisms of cell death

PDT can mediate many signaling events in cells, but its main purpose is to kill cells. The concentration, physical and chemical properties and subcellular location of the PS, a specific wavelength and intensity of light, the concentration of oxygen and cell type-specific properties may influence the mode and extent of cell death[64]. Previous studies shown that cells may undergo two different types of cell death, including necrosis and apoptosis[73].

Necrosis is a violent and quick form of degeneration of cell populations, characterized by a swelling of the cytoplasm, destruction of organelles and disruption of the plasma membrane that leads to a release of intracellular contents and inflammation. Necrosis is caused by physical and chemical damage and is considered an unprogrammed process. The cytoplasmic swelling and progressive disintegration of cytoplasmatic membranes leads to a cellular fragmentation and release of material into the extracellular compartment[64].

Apoptosis is characterized by cell shrinkage and blebbing of the plasma membrane. *In vitro*, apoptotic cells are fragmented into multiple membrane-enclosed spherical vesicles. *In vivo*, apoptotic bodies are eliminated by phagocytes[64].

### 1.3.6 Photodynamic Therapy in Age-related Macular Degeneration: State-of-art

In the area of ophthalmology, PDT has been used in the treatment of neovascular form of AMD (or wet AMD), in which CNV develops under the retina[74]. It has been also used in CNV associated with several retino-choroidal diseases, such as choroiditis and angioid streaks, and diseases without any CNV, like choroidal hemangioma and chronic central serous chorioretinopathy. Promising results in animal models of CNV led to the human clinical trials of three photosensitizing agents: verteporfin, a benzoporphyrin derivative, purlytin, a tin ethyl etiopurpurin and Lu-tex, a lutetium texaphyrin[75]. Due to its absorption spectrum, lipophilic characteristics and short serum half-life, Verteporfin emerged as an optimal agent[76].

Verteporfin accumulates in abnormal neovascular endothelial cells due to their increased expression of low-density lipoprotein (LDL) receptors when in comparison with normal choroidal and retinal vessels. Verteporfin is administered as a liposomal formulation. The use of far-red wavelength light grants a good penetration through melanin, blood and fibrotic tissue allowing an effective treatment of pigmented or haemorrhage lesions located within the choroid[71].

Verteporfin is excited from its ground state to a higher energy state when irradiated with light. The activated verteporfin molecule interacts with oxygen and/or biological substrates, resulting in the creation of cytotoxic singlet oxygen and free radicals. Photodynamic therapy produces vascular endothelial cell damage that results in platelet aggregation, microvascular occlusion and activation of the clotting cascade. The efficacy and selectivity of this therapy for choroidal vascular lesions are dependent on several factors, such as verteporfin dosage, duration of verteporfin infusion and light dose delivered[71].

CNV is characterized by an excessive growth of blood vessels caused by an increase in the production of vascular endothelial growth factors. PDT selectively target and block these new blood vessels. After PDT treatment, there is an increase of angiogenesis, but if used in combination with an anti-VEGF drug, the enhanced angiogenesis is avoided. These treatments can be monitored by using OCT, which allows the identification of the disease morphology[77,787,9].

## 1.4 Aims of the study

AMD is a condition that affects mainly older people and involves the loss of the central field of vision due to the development of lesions in the macula of the retina. AMD can progress to two main advanced subtypes: dry and wet AMD. Recent studies have shown that subretinal fibrosis is present in the advanced stages of AMD, as a wound healing response after damage of photoreceptors and RPE and CNV. Moreover, galectin-1 and -3 have recently shown to play a key role both in CNV development and fibrosis in AMD[16,18]. Although there are some treatments able to retard the progress of the disease, such as intravitreous anti-VEGF drugs, laser photocoagulation, photodynamic therapy, there is no cure for this disease. Thus, the development of therapeutic strategies that could be effective for both CNV and subretinal fibrosis would be of great interest.

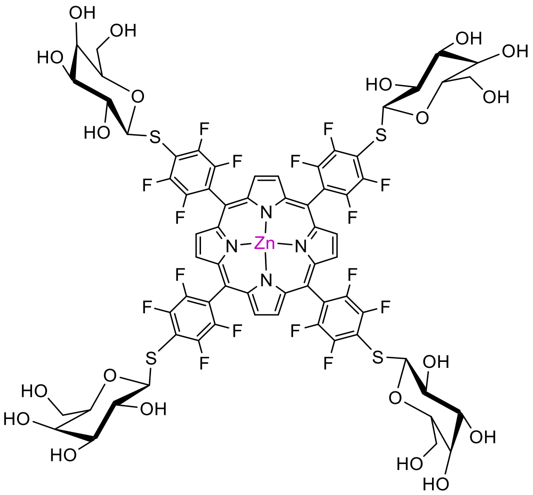

**Figure 7. Chemical structure of a porphyrin with a zinc metal atom in the core, conjugated with four molecules of galactose, ZnTPPF$_{16}$(SGal)$_4$.**

Based on the innate capacity of Exo to communicate with cells, the encapsulation of a photosensitizer in Exo could offer an interesting strategy to deliver the cargo to the fibrous tissue and new vessels of choroid in wet AMD.

The main goal of this work was to develop a novel strategy, based on Exosome-porphyrin nanoformulations to enhance AMD PDT efficacy. For that, we tested the galacto-PS $ZnTPPF_{16}(SGal)_4$ which could eventually be recognized by the overexpressed galectin proteins in advanced AMD, versus its Exosomal form.

Based on this, the main specific objectives of this work were:

- Study the optical absorption spectrum of Zn-porphyrin conjugated with 4 thiogalactose molecules, $ZnTPPF_{16}(SGal)_4$.
- Characterize the exosomes isolated from conditioned media of ARPE-19 cells and from the media bathing the RPE surface of porcine eyecups.
- Assess $ZnTPPF_{16}(SGal)_4$ encapsulation efficiency and integrity of the vesicles.
- Determine the cellular uptake of $ZnTPPF_{16}(SGal)_4$ and exosomal $ZnTPPF_{16}(SGal)_4$.
- Assess the cytotoxicity of $ZnTPPF_{16}(SGal)_4$ and exosomal $ZnTPPF_{16}(SGal)_4$ in darkness and after light irradiation.

# Chapter 2 – Materials and methods

## 2.1 Preparation of $ZnTPPF_{16}(SGal)_4$ working solution

A zinc porphyrin conjugated with 4 units of galactose ($ZnTPPF_{16}(SGal)_4$) was synthesized and characterized by Professor Dr. João Tomé team at the Centro de Química Estrutural (CQE), Departamento de Engenharia Química, Instituto Superior Técnico, Universidade de Lisboa, Portugal.

Stock solutions of $ZnTPPF_{16}(SGal)_4$ at a concentration of 10 mM were prepared in dimethyl sulfoxide (DMSO, Sigma Ref. D4540). After solubilization in an ultrasonic bath (Bandelin Sonorex TK52) for 30 min, stock solutions were stored at -20 ºC, in dark conditions. Freshly working solutions were prepared from the stock solution in sterile phosphate-buffered saline (PBS, 137 mM NaCl, 27 mM KCl, 81 mM $Na_2HPO_4$, 15 mM $KH_2PO_4$, pH 7.40). The concentration of DMSO was always kept less than 0.5% (v/v), in the working solutions.

## 2.2 Photosensitizer absorbance

The electronic absorption spectrum of porphyrins exhibits characteristic bands in two distinct regions. The first one is called the Soret or B band and involves the transition from the ground state to the second excited state. Its absorption is between 380-500 nm. The second region is called Q bands and consists of a weak transition from the ground state to the first excited state. Its absorption is between 500-750 nm[80]. Upon formation of metalloporphyrins, the four Q bands in the visible region collapse into essentially two bands, but the Soret band is barely affected[81].

To assess the absorption spectrum of $ZnTPPF_{16}(SGal)_4$ the absorbance was measured on a microplate reader Synergy™ HT (Biotek Instruments) controlled by BioTek's Gen5™ Data Analysis Software, within the wavelength region 350-800 nm.

The absorption spectrum was obtained using $ZnTPPF_{16}(SGal)_4$, diluted in DMSO and PBS containing 0.5% (v/v) DMSO, at three known concentrations (2, 20 and 50 µM). In a 96-well plate (Orange Scientific), 100 µL of each concentration was added and the absorbance was read.

## 2.3 Maintenance of ARPE-19 cell line

The human RPE cell line ARPE-19 was obtained from the American Type Culture Collection (ATCC number: CRL-2302™). This cell line spontaneously arising from retinal pigment epithelial (RPE) was derived in 1986 from the normal eyes of a 19-year-old male.

ARPE-19 cells grown in monolayer were cultured in complete Dulbecco's Modified Eagle Medium (DMEM)-F12 (ATCC, Ref. ATCC-30-2006), with 10% (v/v) heat-inactivated

Fetal Bovine Serum (FBS; Gibco, Ref. 26140-079) and 1% (v/v) antibiotic/antimycotic containing penicillin, streptomycin and amphotericin B (Gibco, Ref. 15400-062), at 37 ºC in a humidified atmosphere with 5% $CO_2$ and 95% air. Cells were subcultured one to two times a week when they reached approximately 90% of confluence.

### *Defrosting cells*

The ARPE-19 cell line was frozen in 1 mL (containing 10% DMSO) in cryotubes and stored at -80 ºC. The cryotube was thawed, as fast as possible, in a 37 ºC water bath and transferred to 6 mL of pre-warmed DMEM-F12 medium (ATCC, Ref. ATCC-30-2006). After centrifugation at 1500 rpm for 5 minutes, the cell suspension was added to 75 $cm^2$ cell culture flasks. Cells were grown in monolayer at 37 ºC in a humidified incubator gassed with 5% carbon dioxide and 95% air.

### *Subculturing cells*

After a week, the ARPE-19 cell layer was normally confluent, and subculturing was necessary.  The culture medium was removed from the culture flask and discarded. The cell monolayer was washed with warmed sterile PBS twice, in order to remove traces of serum which would inhibit the action of trypsin. The cells were treated with Trypsin (Gibco, 25300-062) and incubated at 37 ºC, 5% $CO_2$ and 95% air, for 5 minutes. The trypsinization progress was monitored under an inverted microscope. The cells were then placed in DMEM-F12 medium. The cell suspension was centrifuged for 5 minutes at 1500 rpm. A pellet was formed at the bottom and the supernatant was discarded. The pellet was resuspended in complete DMEM-F12 medium and aliquots of cells were added to new 75 $cm^2$ culture flasks. ARPE-19 cells were subcultivated at a ratio of 1:3 to 1:5 in the conditions described above. To count cells, 20 µL of the cell suspension was removed and placed in an Eppendorf with 20 µL of blue dye (Lonza, Ref. 17-942E). A mixture of cells (1:1) with blue dye is placed on a Neubauer haemocytometer counting chamber and the number of cells in each quadrant is counted.

### *Freezing cells*

To freeze cells, we resuspend the pellet (obtained as already described) in Fetal Bovine Serum (FBS; Gibco, Ref. 26140-079) (1 mL per stock). In a cryogenic tube, 900 µL of cells were placed with 100 µL of DMSO and stored at -80 ºC.

## 2.4 Isolation of exosomes

### 2.4.1 Isolation of ARPE-19 cell-derived exosomes

As a first approach, we used ARPE-19 cells as a source of exosomes and ultracentrifugation as exosomes isolation method.

ARPE-19 cells were seeded at a density of 3 x $10^5$ cells/ 100-mm cell culture dish (Orange Scientific) and cultured in DMEM-F12 medium at 37 ºC and with 5% $CO_2$ and 95% air, until reach a confluency of 90%. Then, cells were cultured in 7 mL of fresh exofree medium (medium with exosome-depleted FBS). After 12 h, secreted exosomes were isolated from medium by ultracentrifugation. The medium was collected and centrifuged at 300 x *g*, for 10 min. The resulting supernatant was centrifuged at 16000 x *g* (Sigma 3k30), 4 ºC, for 20 minutes. After being filtered with a 0.22 µm filter syringe (Frilabo, Ref. 1520012), the supernatant was ultracentrifuged (Thermo Electron Corporation, Sorvall WX Ultra Series) at 120000 x *g* for 70 min, at 4ºC. The supernatant was discarded, and the pellet was resuspended in PBS for Nano Tracking Analysis (NTA) and Transmission Electron Microscopy (TEM) or RIPA for Western blot analysis.

### 2.4.2 Isolation and purification of RPE cell-derived exosomes from porcine eyecups

A second method for isolate exosomes was performed. Exosomes derived from porcine eyecups were isolated using a commercially available exosome isolation kit (Total Exosome isolation, Invitrogen, Ref. 4478359). For the incubation of the photosensitizer with exosomes, we used these exosomes isolated from porcine eyecups. The porcine eyes were harvested in Matadouro da Beira Litoral, SA, Aveiro, Portugal. The eyecups were incubated with FBS exofree 1% (v/v) medium for 30 minutes and then centrifuged (Reagente 5, Universal 320 R) at 300 x *g* for 10 minutes. Then a new centrifugation (Eppendorf, Centrifuge 5810R) was carried out at 2000 x *g* for 30 minutes, at 4 ºC. A mixture containing 1 mL of supernatant and 0.5 mL of Total Exosome isolation kit (Invitrogen, Ref. 4478359) was incubated overnight at 4 ºC. The next day the samples were centrifuged for 1 hour, at 10000 x *g*, at 4 ºC. The pellet was resuspended in PBS. After isolation, the RPE exosome samples were filtered using a 0.22 µm syringe filter (Filtres Fioroni, Ref. 6002S13001) and subsequently frozen at -20 ºC until use.

## 2.5 Exosome loading with $ZnTPPF_{16}(SGal)_4$

To choose the best conditions to be tested *in vitro*, several conditions were performed in which the number of exosomes (5 to 20 µL of exosomes) and the photosensitizer concentration (0 to 50 µM) varied. After optimizing the photosensitizer loading process in exosomes, the two conditions that proved to be the most promising were chosen for the *in vitro* studies.

Exosomes were mixed with $ZnTPPF_{16}(SGal)_4$ in PBS. After sonication in an ultrasonic bath for 30 minutes, the sample was concentrated and purified using a Centricon (Aicon® Ultra, Merck Millipore, Ref. UFC201024, with a cut-off of 10 kDa), by centrifugation (Eppendorf, Centrifuge 5810R) at 7500 x *g* for 30 minutes. The samples were washed twice in PBS to remove free PS. To recover concentrated sample, a 1000 x *g* centrifugation was performed for 2 minutes. Exosomal $ZnTPPF_{16}(SGal)_4$ was kept at 4ºC.

## 2.6 Determination of fluorescence and absorbance of the exosomal $ZnTPPF_{16}(SGal)_4$

To determine the fluorescence of the exosomal $ZnTPPF_{16}(SGal)_4$, each sample was prepared in PBS (pH 7.40) containing 1% (m/v) sodium dodecyl sulfate (SDS; Biorad, Ref. 161-0301). Fluorescence was measured using the excitation and emission filters at 360/40 nm and 645/40 nm, respectively. To determine absorbance, a sample with PBS was placed in a 96-well plate. The absorbance was measured on a microplate reader Synergy™ HT (Biotek Instruments) controlled by BioTek's Gen5™ Data Analysis Software, between 350-800 nm wavelength. The graphs were obtained using GraphPad Prism (v.8.00, GraphPad Software).

## 2.7 Determination of total protein concentration

The protein concentration in cell extracts was measured spectrophotometrically using the BCA assay kit (BCA/Smith assay; Pierce, Ref. 23227) using bovine serum albumin as a standard in a 96-well plate (Orange Scientific). This method involves two steps. The first step is the biuret reaction in an alkaline environment, whose blue color results from the reduction of cupric ion ($Cu^{2+}$) to cuprous ion ($Cu^{+}$) by peptide bonds in protein. The second step is the chelation of two molecules of BCA with one cuprous ion using the reagent containing bicinchoninic acid, resulting in a water-soluble complex product with a purple color, with a strong absorbance at 562 nm.

For the determination of total protein concentration in PBS pH 7.0 containing 1% SDS , the following solutions were pipetted to each well of a 96-well plate: 25 µL of the sample buffer (sodium dodecyl sulfate (SDS) 1% (m/v) (Biorad, Ref. 161-0301) in PBS (pH 7.0)); 25 µL of sample, blank (sample blank), BSA standard (prepared in the sample buffer at concentration ranging from 12.5 to 800 µg.mL$^{-1}$ prepared from the BSA standard at 2 mg.mL$^{-1}$ and 200 µL of BCA reagent (prepared in 50 parts of reagent A mixed with one part of reagent B). The plate went to the incubator at 37 ºC for 30 minutes. The absorbance at 570 nm was measured on a microplate reader (Synergy HT, Biotek).

Determination of total protein concentration in RIPA was similar to the above mentioned protocol. The difference is that the samples were diluted in RIPA buffer 1:9 (v/v). (RIPA buffer: 150 mM NaCl, 50 mM Tris base, 5 mM EGTA, 0.5% (m/v) DOC, 0.1% (m/v) SDS, 2mM PMSF, 2mM IAD, 1x protease inhibitor cocktail, pH 7.5).

The protein concentration in the samples was directly obtained by plotting the average of the absorbance at 570 nm for each BSA standard in function of its concentration (µg.mL$^{-1}$)[82].

## 2.8 Treatment of ARPE-19 cells with $ZnTPPF_{16}(SGal)_4$ and exosomal $ZnTPPF_{16}(SGal)_4$

Cells were seeded with a density of 3 x $10^4$ cells *per* well, in a 96-well plate for 24 h at 37 ºC and with 5% $CO_2$ and 95% air. One day after seeding the cells into 96 well plates, the culture medium was removed, cells were washed with PBS and incubated with freshly prepared $ZnTPPF_{16}(SGal)_4$ (0.5 and 10 µM) in PBS or exosomal $ZnTPPF_{16}(SGal)_4$ (2, 5 and 10 µL of the mixture purified in section 2.5). We have chosen the conditions, in which mixtures of 10 µL Exosomes: 50 µM $ZnTPPF_{16}(SGal)_4$ and 20 µL Exosomes: 50 µM $ZnTPPF_{16}(SGal)_4$ were performed. The concentration of DMSO was always kept lower than 0.5% (v/v), in all working solutions. The cells were incubated with $ZnTPPF_{16}(SGal)_4$ from 0.5 to 4 hours and with exosomal $ZnTPPF_{16}(SGal)_4$ for 1 hour. Triplicates or quadruplicates of each condition were considered in the assay.

## 2.9 Determination of intracellular photosensitizer concentration by fluorimetry

Due to the fluorescence properties of the porphyrin $ZnTPPF_{16}(SGal)_4$, its amount accumulated in ARPE-19 cells or exosomes was determined by fluorimetry, in which a normalization to total protein quantity is performed.

After $ZnTPPF_{16}(SGal)_4$ or exosomal $ZnTPPF_{16}(SGal)_4$ incubation, cells were washed twice with sterile PBS (100 µL). Cells were then lysed with 120 µL of 1% (v/v) SDS in PBS (pH 7.0). The 96-well plate was placed on the shaker for 30 minutes, at room temperature and in the dark. Ninety µL of cell lysate was placed in a 96-well black bottom plate and fluorescence was measured. The excitation and emission filters used were 360/40 nm and 645/40 nm, respectively.

The ZnTPPF$_{16}$(SGal)$_4$ cellular uptake graph was directly obtained by plotting the average of the fluorescence for the PS standard in function of its concentration using GraphPad Prism (v.8.00, GraphPad Software).

### 2.10 Photodynamic assays

Two of the requirements for an optimal photosensitizing agent are the absence or low dark toxicity and toxicity under suitable irradiation. Therefore, it is important to evaluate the PS toxicity in the absence of light and after irradiation with light at appropriate wavelengths. The excitation of a PS with light irradiation at a specific wavelength induces the production of ROS, which is responsible for cell toxicity.

After incubation with the PS, as described above (section 2.8), cells were washed with PBS and covered with fresh DMEM-F12 medium. Cells were incubated in dark conditions or irradiated with white light for 40 minutes with a LED array system (Fig. 8). The emitted light power was 8.4 mW.cm$^{-2}$. After irradiation, the cells were incubated for 24 hours at 37 ºC and with 5% CO$_2$ and 95% air.

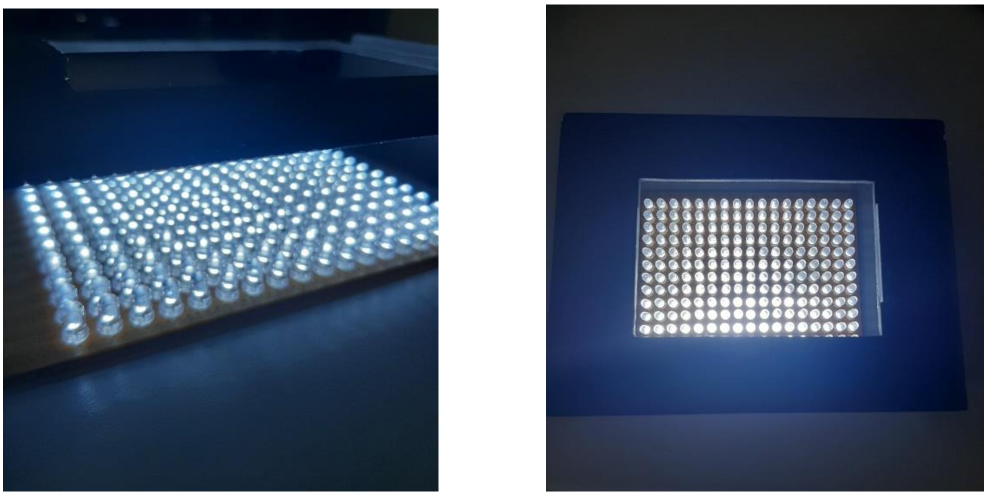

**Figure 8. Representative images of the LED array system.** It is composed of a matrix of 17 x 11 LEDs totalizing 187 light sources emitting white light, with two emission peaks at λ= 450 ± 20 and λ= 550 ± 50 nm.

## 2.11 MTT colorimetric assay

The MTT colorimetric assay is used for measuring cell metabolic activity, as an indicator of cell viability, proliferation and cytotoxicity. The yellow tetrazolium MTT is reduced by metabolically active cells, in part by the action of dehydrogenase enzymes, to purple formazan that is solubilized and quantified by spectrophotometric means.

Cytotoxic effect of $ZnTPPF_{16}(SGal)_4$ or exosomal $ZnTPPF_{16}(SGal)_4$ was evaluated after incubation with $ZnTPPF_{16}(SGal)_4$ and treatment (dark or irradiated – section 2.10), by MTT assay. Twenty-four hours after treatment, 150 µL of DMEM-F12 medium was removed (from 200 µL) and 10 µL of 3 mg/mL MTT (3-[4,5-dimethylthiazol-2-yl]-2,5-diphenyl-tetrazolium bromide) (Sigma, Ref. M2128-1G) was added to each well. The plates were incubated in the darkness for 4h, at 37 ºC and with 5% $CO_2$ and 95% air.

Two hundred µL of acidic isopropanol (0.04 M in pure isopropanol) was added to each well. To solubilize completely the converted dye, repetitive pipetting was applied. The plate was placed on the shaker for a few seconds.

The absorbance was measured at 570 nm (using 620 nm as the background wavelength), using a microplate reader (Synergy HT, Biotek). The data were expressed as a percentage of control (untreated cells)[83].

$$MTT\ reduction\ (\%) = \frac{(absorbance\ treated\ wells)}{(absorbance\ control\ wells)}\ x\ 100\%$$

The MTT reduction graphs in function of time were obtained using GraphPad Prism, GraphPad Software, as well as for the statistical analysis

## 2.12 Western Blotting

Western Blotting is a technique used to detect and quantify specific proteins. A mixture of proteins is separated based on molecular weight through SDS-PAGE[84]. The separated proteins in the gel are electrotransferred to a membrane. Then, incubation of the membrane with primary antibodies serve to detect the proteins of interest.

To run Western Blot, the isolation of exosomes from medium of the cell line ARPE-19 and eyecups was performed as previously described (sections 2.4.1 and 2.4.2). Exosomes resuspended in ice-cold RIPA buffer with fresh protease inhibitors were left on ice for 1 h. The samples were vortexed (VWR) every 10 min and sonicated (Sonics and Materials, Inc) 6 pulses x 3s each. The samples were denatured with Laemmli buffer 5x and heated for 5 min at 95 ºC. The denatured samples were stored at -20 ºC until use.

Fifteen µL of protein samples was loaded on 10% and 12% polyacrylamide gels and the proteins were separated by electrophoresis. The gels were run with low voltage for stacking gel, to line up all the protein samples loaded on the gel, and higher voltage for resolving gel, to separate the proteins based on their molecular weight. The electrophoresis ran until the dye front runs off the bottom of the gel.

In the electrotransfer, the separated protein mixtures were transferred to polyvinylidene difluoride membranes (PDVF; Immun-Blot PVDF membranes, Biorad)), which were previously activated in methanol, and then soaked in Milli-Q water and equilibrated in transfer buffer.

It was created a transfer sandwich with sponges, filters, gel and PVDF membrane. All the material used was previously equilibrated in transfer buffer. The separated proteins were transferred to the PDVF membranes, for 90 min under agitation, using ice cold transfer buffer.

Membranes were incubated with blocking buffer (5% (v/v) non-fat milk prepared in Tris buffer saline tween 20 (TBST buffer; 200 mM Tris base, 1500 mM NaCl, 0.1% (v/v) Tween 20, pH 7.6) for 1 h at room temperature with slow agitation. Then, the membranes were incubated with the primary antibody (diluted in the blocking buffer) overnight, on a rotating wheel at 4 ºC. After incubation, the membranes were washed with TBST (3 x 10 min) at room temperature, with agitation. Table 2 shows the primary antibodies used. The appropriate secondary antibody was added, and the membranes were incubated for 1 h at room temperature, under moderate agitation. After incubation with the secondary antibody, the membranes were washed with TBST (3 x 10 min).

For the detection, the membranes were placed on the chemiluminescence detection system Chemi Doc™ WesternC™ controlled by the software Quantity One (proteins side up) and incubated with the substrate solution (1:1 by volume, mixture of luminol/enhancer and peroxide buffer; Immun-Star™ Chemiluminescent Kit, BioRad) and the images were acquired.

**Table 2**. Primary antibodies used in Western Blot assay

| Antibody | Dilution | Supplier |
|---|---|---|
| CD63 | 1:500 | Sicgen |
| Flotillin-1 | 1:500 | Santa Cruz |
| GAPDH | 1:1000 | Sicgen |

## 2.13 Nanoparticle Tracking Analysis (NTA)

Nanoparticle tracking analysis is a technique used for characterization in terms of concentration of particles and particle size distribution of Exo and it is based on the analysis of Brownian motion. The size of each individually tracked particle is calculated, resulting in the determination of their size distribution and concentration.

Exosomes derived from RPE cells (ARPE-19 cells and porcine eyecups) were resuspended in PBS, after which NTA was assessed using NanoSight LM 10 instrument (NanoSight Ltd). Data were processed using NTA 2.2 analytical software.

## 2.14 Transmission Electron Microscopy (TEM)

Transmission electron microscopy is a technique used to observe the features of very small specimens. It allows the observation of features like ultrastructure and morphology of the cells. Exosomes isolated from porcine eyecups and exosomal $ZnTPPF_{16}(SGal)_4$ were assessed by TEM. Exosomes were fixed with 4% paraformaldehyde, in a mixture 1:1 and deposited on Formvar-carbon coated grids (TAAB Laboratories Equipment). Grids were contrasted with uranyl acetate for 5 minutes. Observations were carried out under TECNAI G2 Spirit BioTWIN electron microscope (FEI) at 100 kV.

# Chapter 3 – Results

## 3.1 Photophysical properties of $ZnTPPF_{16}(SGal)_4$

The absorption spectrum of $ZnTPPF_{16}(SGal)_4$ shows bands characteristics of porphyrins class, with an intense Soret band around 420 nm and another less intense Q-band at a higher wavelength (550 nm). Fig. 9 shows a representative absorption spectrum of $ZnTPPF_{16}(SGal)_4$ in DMSO and PBS containing 0.5% DMSO.

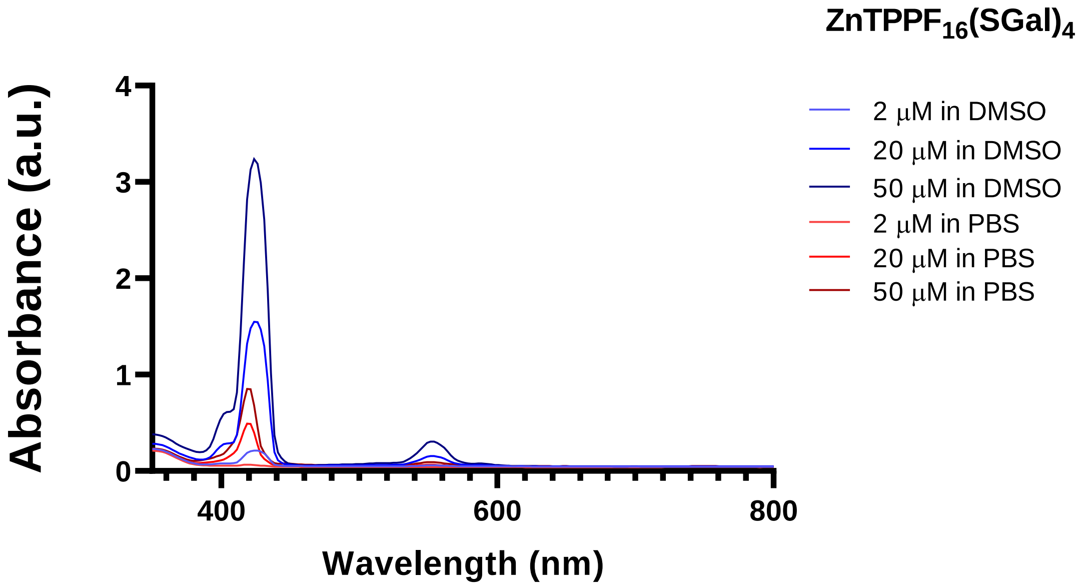

**Figure 9. Electronic absorption spectrum of $ZnTPPF_{16}(SGal)_4$ at 2, 20 and 50 μM in DMSO and in PBS with 0.5% DMSO.**

## 3.2 Characterization of RPE-derived exosomes

As a first approach, exosomes were isolated from the medium of ARPE-19 cell line which, when cultured under specific conditions, presents morphology reminiscent of fibroblasts[85]. The resulting vesicles were characterized by NTA and Western Blotting. NTA revealed that the exosomes recovered by ultracentrifugation from the cell medium of ARPE-19 cells have an average size around 92 nm and the mode was around 120 nm (data not shown). The presence of the tetraspanin CD63 and flotillin, which are common protein markers of exosomes, confirmed that the isolation procedure used gave rise to a population of vesicles enriched in exosomes (Fig. 10A).

Since the number of particles/frame in NTA was relatively low and in the following experiments of PS loading, we needed a high concentration of Exo, we decided to use a commercially available exosome isolation kit, instead of ultracentrifugation procedure. We hypothesized that exosomal recovery from cell media would be greater using this approach compared to ultracentrifugation. In addition, we opted to use porcine eyecups, in which we removed the neuroretina and exposed RPE layer, as a source of exosomes. As expected, we found that CD63 and flotillin-1 were also detected in exosomes from porcine eyecups (Fig. 10B). NTA analysis showed that particles released from RPE of eyecups have a size average and mode of around 142 nm and 123 nm, respectively (Fig. 10C). Moreover, the vesicles visualized by TEM showed a cup-shaped morphology, characteristic of exosomes (Fig. 10D).

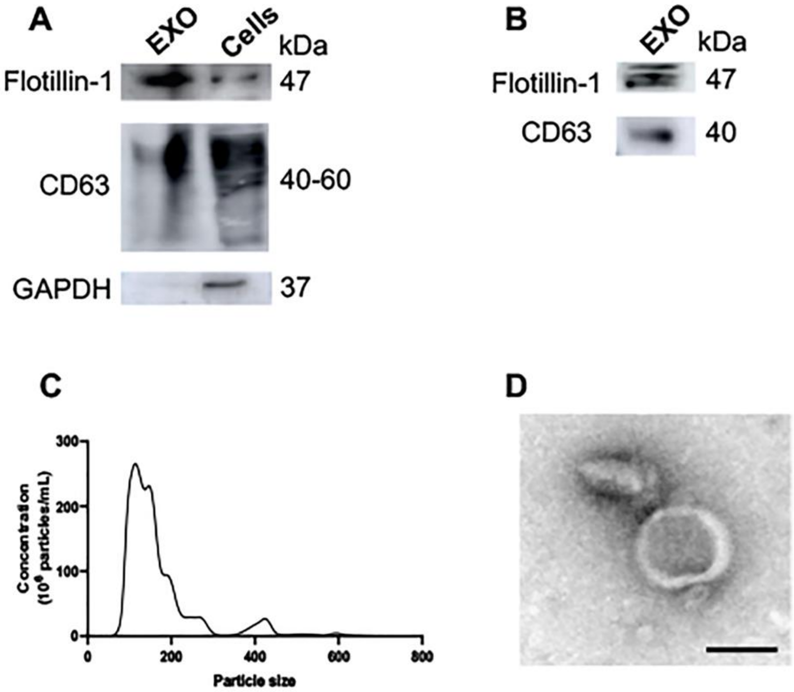

**Figure 10. Characterization of exosomes isolated from ARPE-19 cells and porcine eyecups.** (A) Exosomes were isolated from ARPE-19 cells by ultracentrifugation and Western blot analysis of exosomes and cell lysates was performed to assess the presence of exosomal markers Flotillin-1, CD63 and GAPDH. (B) Western blot analysis of exosomes, isolated using a kit, was performed to assess the presence of the exosomal markers Flotillin-1 and CD63. (C) Representative graph of nanoparticle tracking analysis of eyecup exosomes. A pool of six eyecups was used to perform this analysis. (D) TEM was performed in RPE-derived exosomes from porcine eyecups; Scale bar 100 nm.

### 3.3 Incorporation of ZnTPPF$_{16}$(SGal)$_4$ into exosomes

To assess the ability of exosomes to deliver ZnTPPF$_{16}$(SGal)$_4$, we generated exosomal ZnTPPF$_{16}$(SGal)$_4$. For that, the PS was mixed with eyecups-derived exosomes and then subjected to sonication bath. Different proportions of eyecups-derived exosomes and PS were tested. Concentrations of ZnTPPF$_{16}$(SGal)$_4$ varied between 12.5 and 50 µM. The ZnTPPF$_{16}$(SGal)$_4$ that did not become entrapped into exosomes, was removed using a Centricon® (Centrifugal purification device), which has a cut-off of 10 kDa. As the exosomes have a mean size around 120 nm (confirmed by NTA), the exosomes are expected to be retained in the Centricon®, and the PS that is not encapsulated, which has around 1.8 kDa, passed through the filter. Based on the fluorescence properties of the PS, the loading efficiency was determined by fluorescence spectroscopy (Table 4). To determine the loading efficiency, the fluorescence was measured in the reaction after bath sonication and after purification of exosomes using the Centricon® (Table 3). The calibration curve of fluorescence intensity *versus* concentration of ZnTPPF$_{16}$(SGal)$_4$ is shown in Figure 11.

**Table 3. ZnTPPF$_{16}$(SGal)$_4$ fluorescence intensity before and after purification**

| Conditions | Fluorescence intensity before purification | Fluorescence intensity after purification |
|---|---|---|
| 10 µL Exo | - | - |
| 10 µL Exo + 12.5 µM PS | 9488 | 5154 |
| 10 µL Exo + 25 µM PS | 21922 | 14798 |
| 5 µL Exo + 50 µM PS | 41404 | 15621 |
| 10 µL Exo + 50 µM PS | 42593 | 29587 |
| 20 µL Exo + 50 µM PS | 41507 | 38709 |

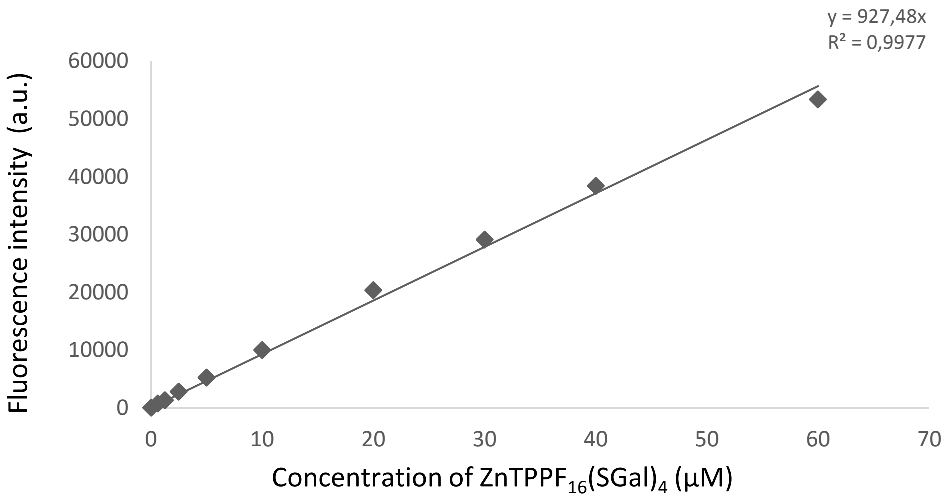

**Figure 11. Calibration curve of fluorescence intensity *versus* concentration of ZnTPPF$_{16}$(SGal)$_4$ from 0 to 60 µM**

**Table 4. ZnTPPF$_{16}$(SGal)$_4$ encapsulation efficiency.**

| Conditions | Quantity of protein (of Exo) (µg) | Volume after purification (µL) | Quantity of final PS/ Quantity of theorical PS x 100 (%) |
|---|---|---|---|
| 10 µL Evs | 20 | 59 | - |
| 10 µL Evs + 12.5 µM PS | 20 | 55 | 30 |
| 10 µL Evs + 25 µM PS | 20 | 55 | 37 |
| 5 µL Evs + 50 µM PS | 10 | 55 | 21 |
| 10 µL Evs + 50 µM PS | 20 | 52 | 36 |
| 20 µL Evs + 50 µM PS | 40 | 54 | 50 |

A high loading efficiency was obtained when a reaction with 20 µL of Exo and 50 µM of PS was performed, with 50% of encapsulation (Table 4). Fig. 12 shows that the intensity of Soret peak (in the absorption spectrum) is also higher in the reaction condition with higher encapsulation efficiency.

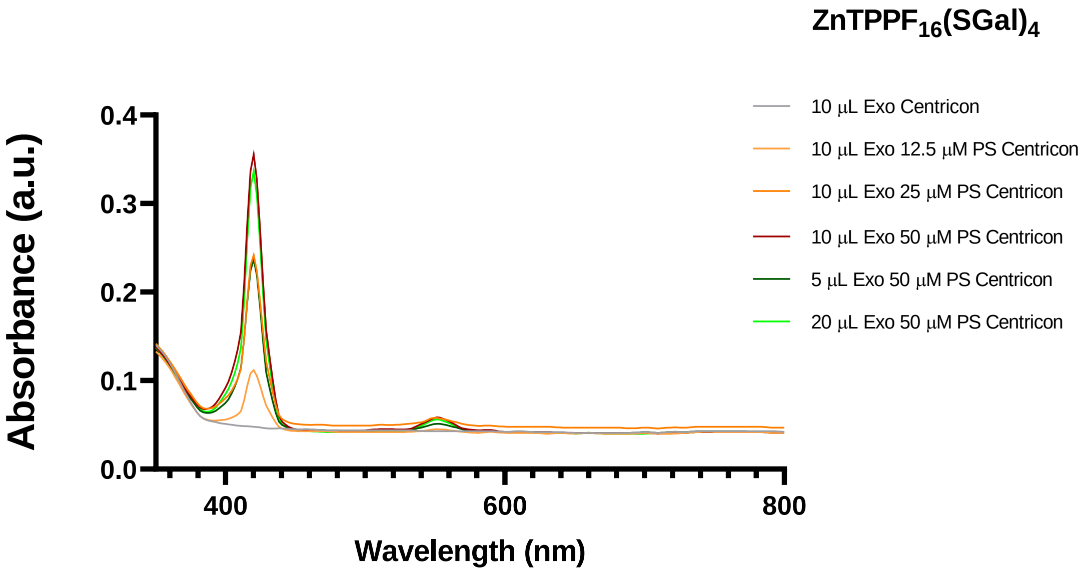

**Figure 12. Absorbance of ZnTPPF$_{16}$(SGal)$_4$ encapsulation.** The absorbance of ZnTPPF$_{16}$(SGal)$_4$ encapsulated in exosomes was measured after purification using centricons.

The TEM analysis showed that free exosomes and exosomal ZnTPPF$_{16}$(SGal)$_4$ present a spheric morphology, with 80-120 nm (Fig. 13). In the latter, the exosomes have darker texture, suggesting encapsulation of electro-dense material, such as ZnTPPF$_{16}$(SGal)$_4$. Moreover, the vesicles did not change their size after incubation with the PS, which is line with PS encapsulation. After the most promising conditions for exossomal ZnTPPF$_{16}$(SGal)$_4$ were chosen, we proceeded to *in vitro* tests.

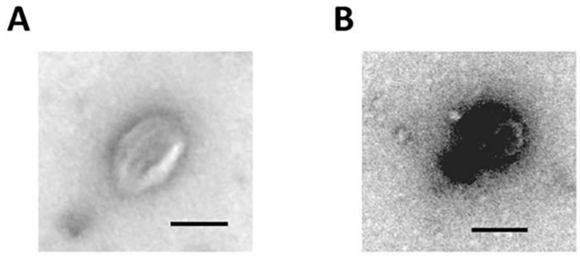

**Figure 13. Transmission electron microscopy (TEM) of exosomes (A) and exosomal $ZnTPPF_{16}(SGal)_4$.** Scale bar 100 nm

### 3.4 Cellular uptake of $ZnTPPF_{16}(SGal)_4$ in ARPE-19 cells

As a first approach, we assessed the amount of free $ZnTPPF_{16}(SGal)_4$ inside of ARPE-19 cells by spectrofluorimetry. ARPE-19 cells were incubated with increasing concentrations of PS (0.5, 1.25, 2.5, 5 and 10 µM) at different times (0.5, 1, 2 and 4 h) in the dark. The intracellular concentration was determined using a calibration curve with known concentrations of the PS (Fig. 14). The cellular uptake of $ZnTPPF_{16}(SGal)_4$ was concentration-dependent and time-dependent up to 2 h of incubation (Fig. 14). We found that when the cells were incubated for 1 h with 10 µM of $ZnTPPF_{16}(SGal)_4$ the intracellular concentration was 5.93 ± 0.81 nmol $ZnTPPF_{16}(SGal)_4$/mg protein (Fig. 14).

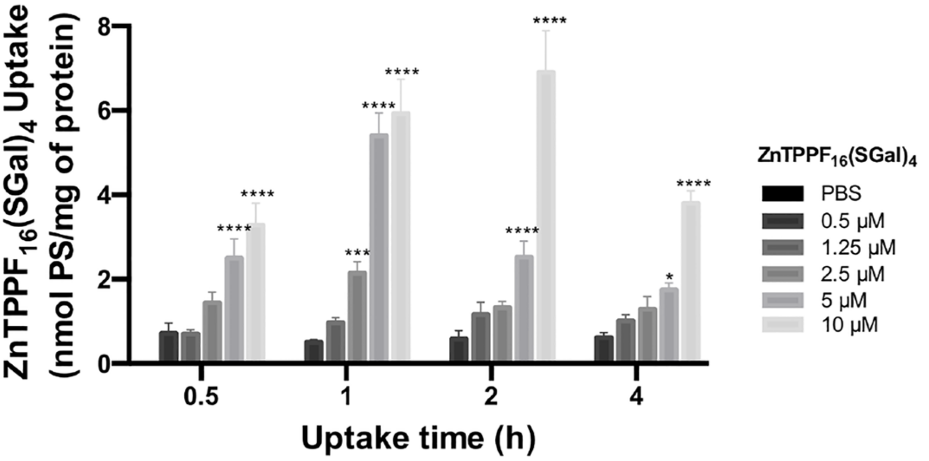

**Figure 14. Intracellular uptake of $ZnTPPF_{16}(SGal)_4$ by ARPE-19 cells**. ARPE-19 cells were incubated in the dark with various concentrations of $ZnTPPF_{16}(SGal)_4$ (0.5, 1.25, 2.5, 5 and 10 µM) for up to 4h. The concentration of $ZnTPPF_{16}(SGal)_4$ was determined using fluorescence spectroscopy and the results were normalized to total protein quantity. Data are the mean ± S.E.M. of three independent experiments performed in triplicates *(p<0.05), ***(p<0.001) and ****(p<0.0001) significantly different from control cells at the same uptake time.

### 3.5 ZnTPPF$_{16}$(SGal)$_4$ induces phototoxicity in ARPE-19 cells

ZnTPPF$_{16}$(SGal)$_4$ cytotoxicity was assessed in the dark and after its photoactivation, 24 h after treatment by MTT assay. No dark toxicity was observed in untreated cells (Fig.15A). The percentage of cytotoxicity was calculated for the control cells, incubated with PBS only. We can see that there was a significant decrease in cell viability when ZnTPPF$_{16}$(SGal)$_4$ was irradiated (using a LED system of white light, at 8.4mW.cm$^{-2}$, for 40 minutes). When the cells were incubated with 10 µM of ZnTPPF$_{16}$(SGal)$_4$ during 0.5, 1, 2 and 4h there was a decrease in the percentage of cell viability of around 82%, 82%, 85% and 92%, respectively.

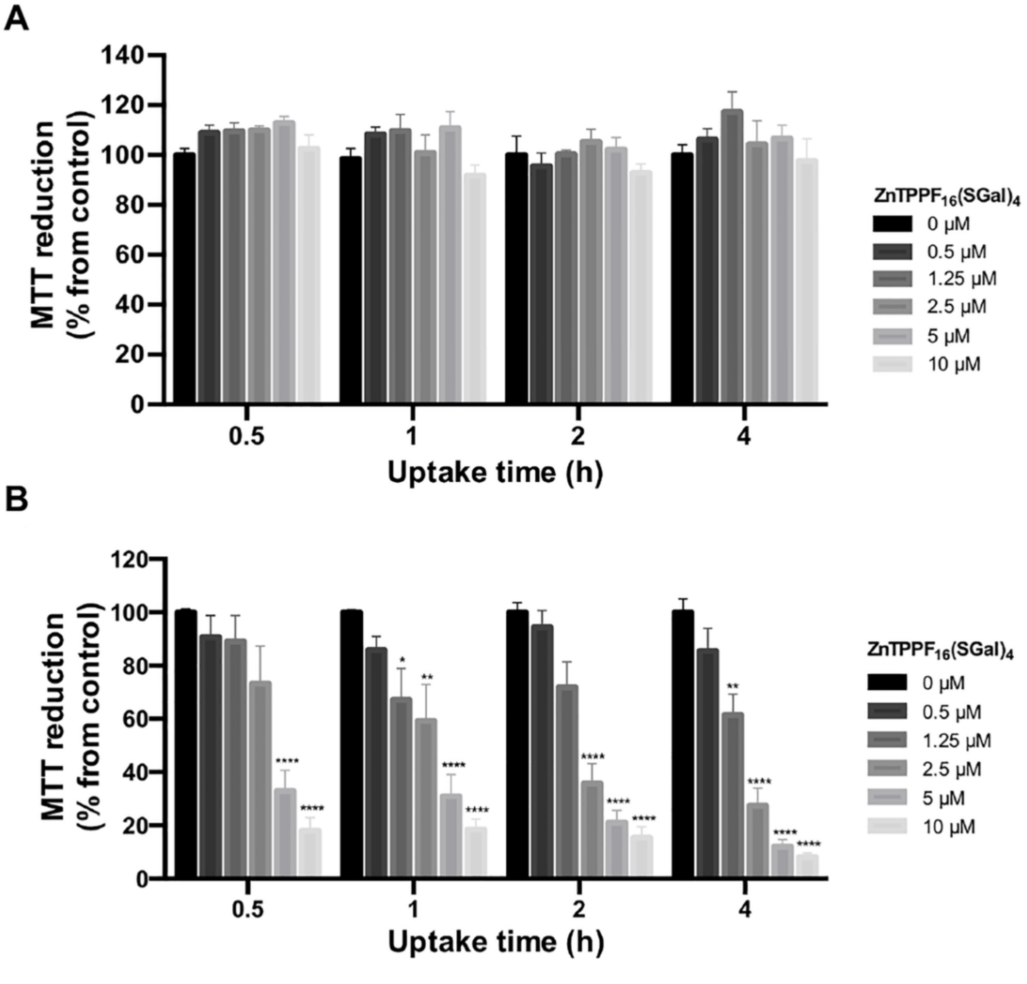

**Figure 15. Toxicity of ZnTPPF$_{16}$(SGal)$_4$ in ARPE-19 cells in dark conditions (A) and after light irradiation (B).** Cells were incubated with ZnTPPF$_{16}$(SGal)$_4$ at various concentrations (0.5, 1.25, 2.5, 5 and 10 µM) for increasing uptake times (0.5, 1, 2, and 4 h) in dark conditions. Cell viability was assessed 24 h after treatment (dark or after irradiation with LEDs at 8.4 mW.cm$^{-2}$ for 40 min) using the using MTT colorimetric assay. The percentage of cytotoxicity was calculated relatively to control cells (cells incubated with PBS) Data are the mean value ± S.E.M. of three independent experiments performed in triplicates. *($p<0.05$), **($p<0.01$) and ****($p<0,0001$) significantly different from control cells at the same uptake time.

### 3.6 Exosomal $ZnTPPF_{16}(SGal)_4$ induces phototoxicity in ARPE-19 cells

After testing $ZnTPPF_{16}(SGal)_4$ in its free form, we next assessed the photodynamic effect of exosomal $ZnTPPF_{16}(SGal)_4$.

For the study of the cytotoxicity of exosomal $ZnTPPF_{16}(SGal)_4$ in ARPE-19 cells, we tested the conditions of 10 and 20 µL of exosomes with 50 µM of the PS, in the dark and after irradiation for 40 min. In these assays, we used different amounts of each purified exosomal $ZnTPPF_{16}(SGal)_4$ solution (2, 5 and 10 µl). The ARPE-19 cells were incubated with different volumes of exosomal $ZnTPPF_{16}(SGal)_4$ and with the compound in the free form, for 1 h, in the dark. Table 5 shows for each condition, the volume used of exosomal $ZnTPPF_{16}(SGal)_4$, and the corresponding amount of the $ZnTPPF_{16}(SGal)_4$ that were used for the *in vitr*o studies. In Table 6 is shown the concentration of $ZnTPPF_{16}(SGal)_4$ and respective quantity of $ZnTPPF_{16}(SGal)_4$ to facilitate the correlation of exosomal $ZnTPPF_{16}(SGal)_4$ quantity with free $ZnTPPF_{16}(SGal)_4$ quantity.

**Table 5. Amount of exosomal $ZnTPPF_{16}(SGal)_4$ and corresponding $ZnTPPF_{16}(SGal)_4$ concentrations.**

| | Exo (µL) | Exo (µg) | Quantity of PS (nmol) |
|---|---|---|---|
| A | 2 | 0.39 | - |
| 10 µL Exo | 5 | 0.98 | - |
| | 10 | 1.96 | - |
| B | 2 | 0.78 | - |
| 20 µL Exo | 5 | 1.96 | - |
| | 10 | 3.91 | - |
| C | 2 | 0.39 | 0.06 |
| 10 µL Exo + 50 µM PS | 5 | 0.98 | 0.16 |
| | 10 | 1.96 | 0.32 |
| D | 2 | 0.78 | 0.08 |
| 20 µL Exo + 50 µM PS | 5 | 1.96 | 0.21 |
| | 10 | 3.91 | 0.42 |

**Table 6. $ZnTPPF_{16}(SGal)_4$ concentration and respective quantity of $ZnTPPF_{16}(SGal)_4$.**

| PS concentration (µM) | Quantity of PS (nmol) |
|---|---|
| 0.5 | 0.03 |
| 1.25 | 0.06 |
| 2.5 | 0.13 |
| 5 | 0.25 |
| 10 | 0.5 |

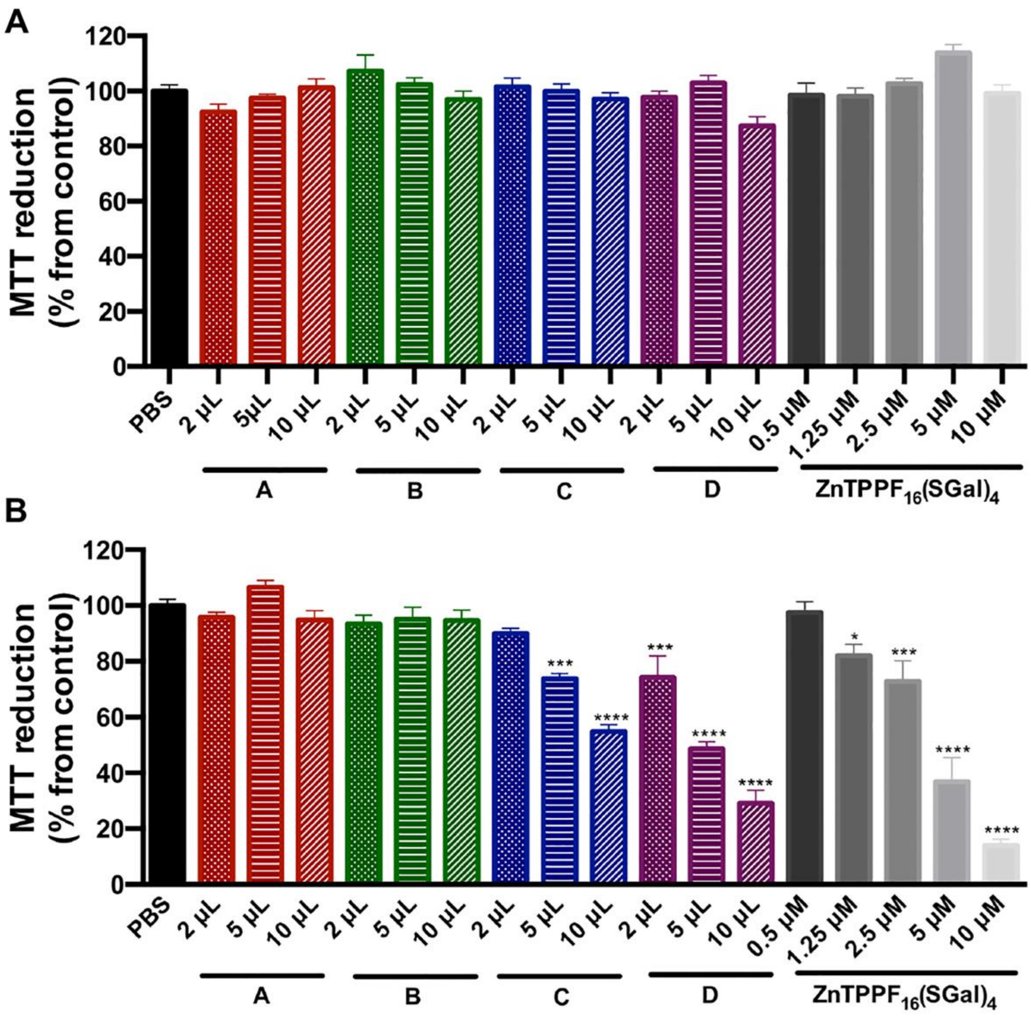

**Figure 16. Exosomal ZnTPPF$_{16}$(SGal)$_4$ is nontoxic in darkness (A) and induces phototoxicity in ARPE-19 cells (B).** Cells were incubated with exosomal ZnTPPF$_{16}$(SGal)$_4$ and free ZnTPPF$_{16}$(SGal)$_4$ at different concentrations (0.5, 1.25, 2.5, 5 and 10 µM) in dark conditions for 1 hour. Cytotoxicity was assessed using MTT colorimetric assay 24 h after treatment. The percentage of cytotoxicity was calculated relatively to control cells (cells incubated with PBS in darkness). Data are the mean value ± S.E.M. of two independent experiments performed in quadruplicates. *(p<0.05), ***(p<0.001) and ****(p<0,0001) significantly different from control cells at the same uptake time.

Cytotoxicity was studied 24 hours after treatment using the MTT colorimetric assay. No dark toxicity was observed in untreated cells (Fig. 16A). However, when cells were incubated with exosomal ZnTPPF$_{16}$(SGal)$_4$ for 1 hour and then irradiated, a significant decrease in cell viability was found in a concentration-dependent manner (Fig. 16B). A quantity of 0.42 nmol of ZnTPPF$_{16}$(SGal)$_4$ (condition D of exosomal ZnTPPF$_{16}$(SGal)$_4$) induced a phototoxicity of approximately 71% and 10 µM free ZnTPPF$_{16}$(SGal)$_4$ (0.5 nmol) shown a phototoxicity of 86.1%.

# Chapter 4 – Discussion

AMD is a common, debilitating eye disease that can cause irreversible vision loss. It is possible to slow down the progression of the disease, but there is currently no cure for AMD. The most common therapies used for wet AMD are inhibitors of VEGF and PDT with the second-generation photosensitizer verteporfin[86]. However, a therapeutic approach that can target both CNV and fibrosis is lacking.

The major goal was to develop a new strategy for improving the AMD management, by targeting fibrosis and CNV. With this in mind, we prepared exosomal $ZnTPPF_{16}(SGal)_4$ with the purpose to improve PDT efficacy. Taking into consideration that extracellular vesicles have the ability to communicate with cells, this strategy could represent a great advantage for the more efficient delivery of the PS to fibroblasts-like and endothelial cells of choroidal neovessels. In this work, we studied a novel galacto-PSs ($ZnTPPF_{16}(SGal)_4$, a zinc porphyrin conjugated with galactose units), which could be recognized by galectin proteins family, and are known to be overexpressed in advanced AMD (in fibrosis and CNV )[16,18].

Although ultracentrifugation is the most commonly used method for isolation of exosomes[87], it has many disadvantages. This is a very time-consuming technique with low purity and there is an aggregation with contaminating proteins. The exosomes yield usually is medium, due to the need for prolonged ultracentrifugation, with the consequent formation of aggregates[28]. Although the exosomes obtained by ultracentrifugation demonstrated the presence of the exosomal markers CD63 and flotillin-1, the NTA analysis revealed a low yield of exosomes, what would be an obstacle to the following steps of the PS encapsulation.

Our group has been already working in exosomes derived from porcine eyecups, isolated through a commercially available exosome isolation kit. So, our approach was to use eyecups as a source of exosomes and perform their isolation through that method. This is a fast and easy procedure, in which no special equipment is needed and, importantly, the exosomes yield is usually high[88]. Although we found a difference in the mean size of exosomes obtained between ultracentrifugation (92 nm) and the exosome isolation kit (140 nm), we found no differences in the mode of particle size between these two isolation methods. This result seems to indicate that the secreted exosomes are mainly derived from RPE cells of porcine eyecups. Although we did not confirm the origin of the secreted exosomes, the content of a RPE marker, such as RPE65, could confirm whether exosomes are mainly derived from RPE cells[7]. We also found a higher yield of exosomes using the isolation kit compared to the ultracentrifugation method.

After confirming the success of exosomes isolation from porcine eyecups, the next step was the choice of a method for encapsulating $ZnTPPF_{16}(SGal)_4$ into exosomes. There are two ways of Exo loading. One is manipulating isolated Exo (exogenous loading) and the other is by acting on parental cells (endogenous loading)[89]. Several approaches for loading therapeutic agents into isolated exosomes have been studied, such as simple vesicle incubation with lipophilic molecules and hydrophobically modified compounds, repeated freezing-thawing procedures, permeabilization with saponin, extrusion, sonication and electroporation[28].

The method used in this study was the sonication bath. In order to establish the best conditions of $ZnTPPF_{16}(SGal)_4$ and exossomal $ZnTPPF_{16}(SGal)_4$ to be used later in *in vitro* tests, we studied six different conditions where we varied the values of Exo between 5 and 20 µL and the PS concentration between 0 and 50 µM. We measured the fluorescence of the six conditions that were not purified and those that were purified. The values of fluorescence intensity for the conditions not purified ranged from 9488 to 42583 and those that were purified ranged from 5154 to 38709. After purification, we choose two of the conditions that seem most promising, $ZnTPPF_{16}(SGal)_4$ at the concentration of 50 µM and the volumes of Exo of 10 and 20 µL. For these two conditions we found consistent fluorescence and absorbance readings. These two conditions had overlapping peaks in the absorbance spectrum that suggests that Exo capacity to encapsulate $ZnTPPF_{16}(SGal)_4$ has reached is maximum. We also did not see any differences between Soret bands of $ZnTPPF_{16}(SGal)_4$ and exossomal $ZnTPPF_{16}(SGal)_4$. After calculating the PS loading efficiency in exosomes, we found that the PS was encapsulated in the Exo in a high percentage comparing to other methods, such as, for example, in the methods used to encapsulate paclitaxel, in which the encapsulation efficiency values were lower in several methods of drug encapsulation[90].

Next, we confirmed by TEM the morphology of the exosomes and exossomal $ZnTPPF_{16}(SGal)_4$. We verified that the vesicles isolated from eyecups exhibited a spherical shape and that the membrane seems to be intact. In exossomal $ZnTPPF_{16}(SGal)_4$ we found that the vesicles are more dense, indicating that the encapsulation of the electro-dense cargo occurred, as is the case of $ZnTPPF_{16}(SGal)_4$. The membrane also appeared not to be disrupted. Although these data seem to indicate the encapsulation of the PS, we cannot conclude whether $ZnTPPF_{16}(SGal)_4$ is inside of exosomes or it is on the exosome membrane surface.

The main purpose of this work was to compare the cellular uptake and phototoxicity induced by $ZnTPPF_{16}(SGal)_4$, in its free form and when encapsulated in exosomes. Therefore, an uptake study was performed with the compound in free form on the ARPE-19 cell line.

In the study of $ZnTPPF_{16}(SGal)_4$ internalization in ARPE-19 cells, we studied four different uptake times and increasing concentrations of PS, from 0.5 to 10 µM, ensuring that DMSO percentage did not exceed 0.5% (v/v), which could interfere with cell viability.

The cellular uptake of the free form of the PS was concentration- and time-dependent up to 2 h of incubation. Interestingly, the cellular uptake decreased after 4h of incubation. This could be due to the technical issues or, eventually, to the activity of efflux transporters. Efflux cell membrane transporters are important in the process of moving the parent drug and metabolites of some medications out of the cell and contribute to drug resistance by decreasing the therapeutic effect that is desired. It has also been reported that when is an up-regulation of efflux cell membrane transporters, it results in the rise of the removal of medication[91]. Models based in the cell line ARPE-19, do not have an appropriate barrier to restrict drug flux across the monolayer but are useful in drug uptake studies[92]. Based on the results obtained, we verified that the best incubation times for $ZnTPPF_{16}(SGal)_4$ were 1 and 2 hours. $ZnTPPF_{16}(SGal)_4$ revealed to be nontoxic in the dark, inducing phototoxicity only after being photoactivated.

The next step was to compare the photodynamic effect between the free $ZnTPPF_{16}(SGal)_4$ and exosomal $ZnTPPF_{16}(SGal)_4$. For the *in vitro* studies, we used the most promising conditions of the exossomal $ZnTPPF_{16}(SGal)_4$ conditions, 10 and 20 µL of exosomes with a PS concentration of 50 µM. To make sure that the integrity of the exossomal $ZnTPPF_{16}(SGal)_4$ was not compromised, they were freshly prepared, purified and incubated on ARPE-19 cell line.

Different volumes of each condition were used for incubation in ARPE-19 cells. Our conditions with exossomal $ZnTPPF_{16}(SGal)_4$ produced phototoxicity, with the condition of 20 µL Exo with a PS concentration of 50 µM having the highest phototoxicity value.

To compare the MTT reduction values, we calculated the quantity of $ZnTPPF_{16}(SGal)_4$ added to the cells. The quantity values added to the cells range from 0.06 to 0.42 nmol. When we compared the MTT reduction values, we found that the exossomal $ZnTPPF_{16}(SGal)_4$ values were not higher compared to the values of free $ZnTPPF_{16}(SGal)_4$, showing that exossomal $ZnTPPF_{16}(SGal)_4$ did not increase the effectiveness of the PS. This means that in the conditions used in our study, there was not an improvement of the efficacy of PDT with exossomal $ZnTPPF_{16}(SGal)_4$ compared to the free PS. Therefore, an optimization of the protocol of encapsulation is needed, as well as a detailed characterization of exosomal cargo. In addition, new methods for Exo encapsulation can be envisioned to improve the efficacy of PDT with exosomal $ZnTPPF_{16}(SGal)_4$.

# Chapter 5 – Conclusion

In this study, we aimed to evaluate the photodynamic effect of a zinc-porphyrin, $ZnTPPF_{16}(SGal)_4$, and exosomal $ZnTPPF_{16}(SGal)_4$ using the ARPE-19 cells, which are fibroblast-like.

Our studies revealed that exosomes isolated from both ARPE-19 cells and eyecups have a similar mode particle size about 120 nm. The two methods of exosomes isolation tested were successful in the isolation of exosomes, as confirmed by NTA, TEM and presence of exosomal markers, flotillin-1 and CD63. The exosomes isolation kit produced higher yield of exosomes than the ultracentrifugation procedure. In addition, using eyecups as a source of exosomes, a high yield of exosomes was obtained.

The method of sonication bath for encapsulation of $ZnTPPF_{16}(SGal)_4$ in exosomes revealed a high encapsulation efficiency, as revealed by the fluorescence and absorbance studies. Analysis of the vesicles morphology by TEM demonstrated an integrity of the vesicles after encapsulation of the PS. Furthermore, the vesicles appearance after encapsulation by TEM was more electron-dense, which supports the encapsulation of electron dense material, such as the porphyrin zinc complex PS.

$ZnTPPF_{16}(SGal)_4$ or exosomal $ZnTPPF_{16}(SGal)_4$ did not induce dark toxicity. Despite both induced phototoxicity in a concentration- and time- dependent manner, there was not an improved photodynamic effect observed when the PS was encapsulated in exosomes.

For the study of photosensitizer encapsulation into Exo, we choose the method of sonication bath. Exosomal $ZnTPPF_{16}(SGal)_4$ have been purified and photophysical studies have been performed, due to our compound optic characteristics. We found that the encapsulation efficiency of this method ranges from 20 to 50% in the conditions performed.

We checked by TEM the morphology of our exosomes with or without $ZnTPPF_{16}(SGal)_4$ (after 30 minutes in the sonication bath), and it seems that the procedures used did not induce a disruption of the membrane of the Exo. Although TEM analysis showed dense areas in the exosomal $ZnTPPF_{16}(SGal)_4$, we cannot know whether PS is encapsulated into the Exo or it is attached to the membrane of the extracellular vesicles.

We verified that before being irradiated, $ZnTPPF_{16}(SGal)_4$ did not induce cytotoxicity, neither in the free form nor encapsulated in the Exo. We also found that Exosomal $ZnTPPF_{16}(SGal)_4$ does not lead to greater phototoxicity after a 40-minute irradiation when compared to free $ZnTPPF_{16}(SGal)_4$.

The study was carried out on ARPE-19 cells, that under specific conditions of culture, can transdifferentiate into fibroblast-like cells through EMT. This approach is relevant in the context of AMD, since subretinal fibrosis can be present. Taken together, the results showed that $ZnTPPF_{16}(SGal)_4$ can be envisaged as a promising photosensitizer for the photodynamic treatment of fibrosis in AMD. Further studies towards therapeutic efficacy for CNV in AMD are warranted.

# Bibliography

1. Wong, W. L. *et al.* Global prevalence of age-related macular degeneration and disease burden projection for 2020 and 2040: A systematic review and meta-analysis. *Lancet Glob. Heal.* **2**, (2014).
2. Ljubimov, A. V. Cell Therapy for Age-Related Macular Degeneration: A New Vision for the Bone Marrow? *Mol. Ther.* **25**, 832–833 (2017).
3. Colijn, J. M. *et al.* Prevalence of Age-Related Macular Degeneration in Europe: The Past and the Future. *Ophthalmology* **124**, 1753–1763 (2017).
4. Smith, W. *et al.* Risk factors for age-related macular degeneration: Pooled findings from three continents. *Ophthalmology* **108**, 697–704 (2001).
5. Mitchell, P., Jin Wang, J., Smith, W. & Leeder, S. R. Smoking and the 5-year incidence of age-related maculopathy: The Blue Mountains Eye Study. *Arch. Ophthalmol.* **120**, 1357–1363 (2002).
6. Zarbin, M. A. Current Concepts in the Pathogenesis of Age-Related Macular Degeneration. *Arch. Ophthalmol.* **122**, 598–614 (2004).
7. Biasutto, L., Chiechi, A., Couch, R., Liotta, L. A. & Espina, V. Retinal pigment epithelium (RPE) exosomes contain signaling phosphoproteins affected by oxidative stress. *Exp. Cell Res.* **319**, 2113–2123 (2013).
8. Heesterbeek, T. J., Lorés-Motta, L., Hoyng, C. B., Lechanteur, Y. T. E. & den Hollander, A. I. Risk factors for progression of age-related macular degeneration. *Ophthalmic Physiol. Opt.* **40**, 140–170 (2020).
9. Mitchell, P., Liew, G., Gopinath, B. & Wong, T. Y. Age-related macular degeneration. *Lancet* **392**, 1147–1159 (2018).
10. Gheorghe, A., Mahdi, L. & Musat, O. Age-Related Macular Degeneration. *Rom. J. Ophthalmol.* **59**, 74–77 (2015).
11. Cicinelli, M. V. *et al.* Optical coherence tomography angiography in dry age-related macular degeneration. *Surv. Ophthalmol.* **63**, 236–244 (2018).
12. Qin, S. Oxidative damage of retinal pigment epithelial cells and age-related macular degeneration. *Drug Dev. Res.* **68**, 213–225 (2007).
13. Cross, M. J. & Claesson-Welsh, L. FGF and VEGF function in angiogenesis: Signalling pathways, biological responses and therapeutic inhibition. *Trends Pharmacol. Sci.* **22**, 201–207 (2001).
14. Hsieh, S. H. *et al.* Galectin-1, a novel ligand of neuropilin-1, activates VEGFR-2 signaling and modulates the migration of vascular endothelial cells. *Oncogene* **27**, 3746–3753 (2008).
15. IMarkowska, A., Cao, Z. & Panjwani, N. Glycobiology of ocular angiogenesis. *Glycobiology* **24**, 1275–1282 (2014).

16. Wu, D. *et al.* Galectin-1 promotes choroidal neovascularization and subretinal fibrosis mediated via epithelial-mesenchymal transition. *FASEB J.* **33**, 2498–2513 (2019).
17. Van Lookeren Campagne, M., Lecouter, J., Yaspan, B. L. & Ye, W. Mechanisms of age-related macular degeneration and therapeutic opportunities. *J. Pathol.* **232**, 151–164 (2014).
18. Little, K., Ma, J. H., Yang, N., Chen, M. & Xu, H. Myofibroblasts in macular fibrosis secondary to neovascular age-related macular degeneration - the potential sources and molecular cues for their recruitment and activation. *EBioMedicine* **38**, 283–291 (2018).
19. Özkiris, A. Anti-VEGF agents for age-related macular degeneration. *Expert Opin. Ther. Pat.* **20**, 103–118 (2010).
20. Mehta, S. Age-Related Macular Degeneration. *Prim. Care - Clin. Off. Pract.* **42**, 377–391 (2015).
21. Lim, L. S., Mitchell, P., Seddon, J. M., Holz, F. G. & Wong, T. Y. Age-related macular degeneration. *Lancet* **379**, 1728–1738 (2012).
22. Al-Zamil, W. M. & Yassin, S. A. Recent developments in age-related macular degeneration: A review. *Clin. Interv. Aging* **12**, 1313–1330 (2017).
23. Yeo, N. J. Y., Chan, E. J. J. & Cheung, C. Choroidal neovascularization: Mechanisms of endothelial dysfunction. *Front. Pharmacol.* **10**, (2019).
24. Abels, E. R. & Breakefield, X. O. Introduction to Extracellular Vesicles: Biogenesis, RNA Cargo Selection, Content, Release, and Uptake. *Cell. Mol. Neurobiol.* **36**, 301–312 (2016).
25. Rashed, M. H. *et al.* Exosomes: From garbage bins to promising therapeutic targets. *Int. J. Mol. Sci.* **18**, (2017).
26. Théry, C., Zitvogel, L. & Amigorena, S. Exosomes: Composition, biogenesis and function. *Nat. Rev. Immunol.* **2**, 569–579 (2002).
27. Batrakova, E. V. & Kim, M. S. Using exosomes, naturally-equipped nanocarriers, for drug delivery. *J. Control. Release* **219**, 396–405 (2015).
28. Villa, F., Quarto, R. & Tasso, R. Extracellular vesicles as natural, safe and efficient drug delivery systems. *Pharmaceutics* **11**, (2019).
29. Cai, J. *et al.* Extracellular vesicle-mediated transfer of donor genomic DNA to recipient cells is a novel mechanism for genetic influence between cells. *J. Mol. Cell Biol.* **5**, 227–238 (2013).
30. Lu, M. & Huang, Y. Bioinspired exosome-like therapeutics and delivery nanoplatforms. *Biomaterials* **242**, 119925. (2020).

31. Huang, S. *et al.* The phylogenetic analysis of tetraspanins projects the evolution of cell-cell interactions from unicellular to multicellular organisms. *Genomics* **86**, 674–684 (2005).
32. Petrovčíková, E., Vičíková, K. & Leksa, V. Extracellular vesicles – biogenesis, composition, function, uptake and therapeutic applications. *Biol.* **73**, 437–448 (2018).
33. Fukushima, A., Takahashi, E., Saruwatari, J., Tanihara, H. & Inoue, T. The angiogenic effects of exosomes secreted from retinal pigment epithelial cells on endothelial cells. *Biochem. Biophys. Reports* **22**, 100760 (2020).
34. Raposo, G. *et al.* B lymphocytes secrete antigen-presenting vesicles. *J. Exp. Med.* **183**, 1161–1172 (1996).
35. Zhang, Y. *et al.* Exosome: A review of its classification, isolation techniques, storage, diagnostic and targeted therapy applications. *Int. J. Nanomedicine* **15**, 6917–6934 (2020).
36. Akers, J. C., Gonda, D., Kim, R., Carter, B. S. & Chen, C. C. Biogenesis of extracellular vesicles (EV): Exosomes, microvesicles, retrovirus-like vesicles, and apoptotic bodies. *J. Neurooncol.* **113**, 1–11 (2013).
37. Zhang, Y., Liu, Y., Liu, H. & Tang, W. H. Exosomes: Biogenesis, biologic function and clinical potential. *Cell Biosci.* **9**, 19 (2019).
38. Meng, W. *et al.* Prospects and challenges of extracellular vesicle-based drug delivery system: considering cell source. *Drug Deliv.* **27**, 585–598 (2020).
39. Raposo, G. & Stoorvogel, W. Extracellular vesicles: Exosomes, microvesicles, and friends. *J. Cell Biol.* **200**, 373–383 (2013).
40. Colombo, M., Raposo, G. & Théry, C. Biogenesis, secretion, and intercellular interactions of exosomes and other extracellular vesicles. *Annu. Rev. Cell Dev. Biol.* **30**, 255–289 (2014).
41. Haraszti, R. A. *et al.* High-resolution proteomic and lipidomic analysis of exosomes and microvesicles from different cell sources. *J. Extracell. Vesicles* **5**, 32570 (2016).
42. Antimisiaris, S. G., Mourtas, S. & Marazioti, A. Exosomes and exosome-inspired vesicles for targeted drug delivery. *Pharmaceutics* **10**(4), 218 (2018).
43. Tran, P. H. L. *et al.* Development of a nanoamorphous exosomal delivery system as an effective biological platform for improved encapsulation of hydrophobic drugs. *Int. J. Pharm.* **566**, 697–707 (2019).
44. Luan, X. *et al.* Engineering exosomes as refined biological nanoplatforms for drug delivery. *Acta Pharmacol. Sin.* **38**, 754–763 (2017).

45. Lim, W. & Kim, H. S. Exosomes as Therapeutic Vehicles for Cancer. *Tissue Eng. Regen. Med.* **16**, 213–223 (2019).
46. Balachandran, B., Yuana, Y. & Schumacher, U. Extracellular vesicles-based drug delivery system for cancer treatment. *Cogent Med.* **6**, 1635806 (2019).
47. Zhao, X. *et al.* Exosomes as drug carriers for cancer therapy and challenges regarding exosome uptake. *Biomed. Pharmacother.* **128**, 110237 (2020).
48. Tominaga, N., Yoshioka, Y. & Ochiya, T. A novel platform for cancer therapy using extracellular vesicles. *Adv. Drug Deliv. Rev.* **95**, 50–55 (2015).
49. Braccioli, L., Van Velthoven, C. & Heijnen, C. J. Exosomes: A new weapon to treat the central nervous system. *Mol. Neurobiol.* **49**, 113–119 (2014).
50. Jiang, X. C. & Gao, J. Q. Exosomes as novel bio-carriers for gene and drug delivery. *Int. J. Pharm.* **521**, 167–175 (2017).
51. Rak, J., Pouckova, P., Benes, J. & Vetvicka, D. Drug delivery systems for phthalocyanines for photodynamic therapy. *Anticancer Res.* **39**, 3323–3339 (2019).
52. Daniell, M. D. & Hill, J. S. a History of Photodynamic Therapy. *Aust. N. Z. J. Surg.* **61**, 340–348 (1991).
53. Kwiatkowski, S. *et al.* Photodynamic therapy – mechanisms, photosensitizers and combinations. *Biomed. Pharmacother.* **106**, 1098–1107 (2018).
54. Kessel, D. Photodynamic Therapy: A Brief History. *J. Clin. Med.* **8**, 1581 (2019).
55. Baldes, E. J. The Photodynamic Properties of a Particular Hematoporphyrin Derivative. *Arch. Dermatol.* **82**, 508–516 (1960).
56. Lipson, R. L., Baldes, E. J. & Olsen, A. M. The use of a derivative of hematoporphyrin in tumor detection. *J. Natl. Cancer Inst.* **26**, 1–11 (1961).
57. Li, X., Kolemen, S., Yoon, J. & Akkaya, E. U. Activatable Photosensitizers: Agents for Selective Photodynamic Therapy. *Adv. Funct. Mater.* **27**, (2017).
58. Capella, M. A. M. & Capella, L. S. A light in multidrug resistance: Photodynamic treatment of multidrug-resistant tumors. *J. Biomed. Sci.* **10**, 361–366 (2003).
59. Kim, J., Jo, Y. um & Na, K. Photodynamic therapy with smart nanomedicine. *Arch. Pharm. Res.* **43**, 22–31 (2020).
60. Allison, R. R. & Moghissi, K. Photodynamic therapy (PDT): PDT mechanisms. *Clin. Endosc.* **46**, 24–29 (2013).
61. Zhang, J. *et al.* An updated overview on the development of new photosensitizers for anticancer photodynamic therapy. *Acta Pharm. Sin. B* **8**, 137–146 (2018).
62. Dolmans, D. E. J. G. J., Fukumura, D. & Jain, R. K. Photodynamic therapy for cancer. *Nat. Rev. Cancer* **3**, 380–387 (2003).

63. Lin, J.-T., Chen, K.-T. & Liu, H.-W. Progress of nanotechnology for phototherapy: Fundamentals and applications. *Med. Devices Diagnostic Eng.* **2**, (2017).
64. Castano, A. P., Demidova, T. N. & Hamblin, M. R. Mechanisms in photodynamic therapy: Part two - Cellular signaling, cell metabolism and modes of cell death. *Photodiagnosis Photodyn. Ther.* **2**, 1–23 (2005).
65. Kessel, D. & Oleinick, N. L. Photodynamic therapy and cell death pathways. *Methods Mol. Biol.* **635**, 35–46 (2010).
66. MOAN, J. & BERG, K. the Photodegradation of Porphyrins in Cells Can Be Used To Estimate the Lifetime of Singlet Oxygen. *Photochem. Photobiol.* **53**, 549–553 (1991).
67. Swavey, S. & Tr, M. Porphyrin and Phthalocyanine Photosensitizers as PDT Agents: A New Modality for the Treatment of Melanoma. *Recent Adv. Biol. Ther. Manag. Melanoma* (2013) doi:10.5772/54940.
68. Gold, M. H. History of Photodynamic Therapy. *Photodyn. Ther. Dermatology* 1–4 (2011) doi:10.1007/978-1-4419-1298-5_1.
69. Yoon, I., Li, J. Z. & Shim, Y. K. Advance in photosensitizers and light delivery for photodynamic therapy. *Clin. Endosc.* **46**, 7–23 (2013).
70. Dougherty, T. J. *et al.* Photodynamic therapy. *J. Natl. Cancer Inst.* **90**, 889–905 (1998).
71. Schmidt-Erfurth, U. & Hasan, T. Mechanisms of action of photodynamic therapy with verteporfin for the treatment of age-related macular degeneration. *Surv. Ophthalmol.* **45**, 195–214 (2000).
72. Bown, S. G. Science, medicine, and the future: New techniques in laser therapy. *Br. Med. J.* **316**, 754–757 (1998).
73. Kerr, J. F. R., Wyllie, A. H. & Currie, A. R. Apoptosis: A basic biological phenomenon with wide-ranging implications in tissue kinetics. *Br. J. Cancer* **26**, 239–257 (1972).
74. Wormald, R., Evans, J., Smeeth, L. & Henshaw, K. Photodynamic therapy for neovascular age-related macular degeneration. *Cochrane Database Syst. Rev.* (2007) doi:10.1002/14651858.CD002030.pub3.
75. Regillo, C. D. Update on photodynamic therapy. *Curr. Opin. Ophthalmol.* **11**, 166–170 (2000).
76. Miller, J., Schmidt-Erfurth, U. & Sickenberg, M. Photodynamic therapy with verteporfin for choroidal neovascularization caused by age - related macular degeneration. *Evidence-Based Eye Care* **1**, 94–95 (2000).

77. Roberts, J. E. Techniques to Improve Photodynamic Therapy. *Photochem. Photobiol.* **96**, 524–528 (2020).
78. Newman, D. K. Photodynamic therapy: Current role in the treatment of chorioretinal conditions. *Eye* **30**, 202–210 (2016).
79. Mennel, S., Barbazetto, I., Meyer, C. H., Peter, S. & Stur, M. Ocular photodynamic therapy - Standard applications and new indications (part 1): Review of the literature and personal experience. *Ophthalmologica* **221**, 216–226 (2007).
80. Giovannetti, R. The Use of Spectrophotometry UV-Vis for the Study of Porphyrins. *Macro To Nano Spectrosc.* (2012) doi:10.5772/38797.
81. Huang, X., Nakanishi, K. & Berova, N. Porphyrins and metalloporphyrins: Versatile circular dichroic reporter groups for structural studies. *Chirality* **12**, 237–255 (2000).
82. Smith, P. K. *et al.* Measurement of protein using bicinchoninic acid. *Anal. Biochem.* **150**, 76–85 (1985).
83. Mosmann, T. Rapid colorimetric assay for cellular growth and survival: Application to proliferation and cytotoxicity assays. *J. Immunol. Methods* **65**, 55–63 (1983).
84. Mahmood, T. & Yang, P. C. Western blot: Technique, theory, and trouble shooting. *N. Am. J. Med. Sci.* **4**, 429–434 (2012).
85. Samuel, W. *et al.* Appropriately differentiated ARPE-19 cells regain phenotype and gene expression profiles similar to those of native RPE cells. *Mol. Vis.* **23**, 60–89 (2017).
86. Debefve, E., Pegaz, B., Ballini, J. P. & Van Den Bergh, H. Combination therapy using verteporfin and ranibizumab; Optimizing the timing in the cam model. *Photochem. Photobiol.* **85**, 1400–1408 (2009).
87. Théry, C., Amigorena, S., Raposo, G. & Clayton, A. Isolation and Characterization of Exosomes from Cell Culture Supernatants and Biological Fluids. *Curr. Protoc. Cell Biol.* **30**, Chapter 3:Unit 3.22. (2006).
88. Kotmakçı, M. & Akbaba, G. E. Exosome Isolation: Is There an Optimal Method with Regard to Diagnosis or Treatment? *Nov. Implic. Exosomes Diagnosis Treat. Cancer Infect. Dis.* (2017) doi:10.5772/intechopen.69407.
89. Wiklander, O. P. B., Brennan, M., Lötvall, J., Breakefield, X. O. & Andaloussi, S. E. L. Advances in therapeutic applications of extracellular vesicles. *Sci. Transl. Med.* **11**(492), (2019).

90. Kim, M. S. *et al.* Development of exosome-encapsulated paclitaxel to overcome MDR in cancer cells. *Nanomedicine Nanotechnology, Biol. Med.* **12**, 655–664 (2016).

91. Giacomini, K. M. *et al.* Membrane transporters in drug development. *Nat. Rev. Drug Discov.* **9**, 215–236 (2010).

92. Hellinen, L. *et al.* Drug flux across RPE cell models: The hunt for an appropriate outer blood–retinal barrier model for use in early drug discovery. *Pharmaceutics* **12**(2),176, (2020).